* Manuscript

Multi-scaled Analysis of the Damped Dynamics of an Elastic Continuum with an Essentially Nonlinear End Attachment

Panayotis Panagopoulos, Fotios Georgiades,
Stylianos Tsakirtzis, Alexander F. Vakakis†
Mechanics Division,
Faculty of Applied Mathematical and Physical Sciences,
National Technical University of Athens,
panago58@otenet.gr, fgeorgia@mail.ntua.gr, tsakstel@central.ntua.gr, vakakis@central.ntua.gr
and
Lawrence A. Bergman
Department of Aerospace Engineering
University of Illinois at Urbana – Champaign
Urbana, Illinois 61801
lbergman@uiuc.edu

† Corresponding author,
P.O.Box 64042, GR-157 10 Zografos, Athens, Greece
Also,
Department of Mechanical and Industrial Engineering (adjunct),
Department of Aerospace Engineering (adjunct),
University of Illinois at Urbana-Champaign, avakakis@uiuc.edu

Abstract

We study multi-frequency transitions in the transient dynamics of a viscously damped dispersive finite rod with an essentially nonlinear end attachment. The attachment consists of a small mass connected to the rod by means of an essentially nonlinear stiffness in parallel to a viscous damper. First, the periodic orbits of the underlying hamiltonian system with no damping are computed, and depicted in a frequency-energy plot (FEP). This representation enables one to clearly distinguish between the different types of periodic motions, forming back bone curves and subharmonic tongues. Then the damped dynamics of the system is computed; the rod and attachment responses are initially analyzed by the numerical Morlet Wavelet Transform (WT), and then by the Empirical Mode Decomposition (EMD) or Hilbert-Huang Transform (HTT), whereby, the time series are decomposed in terms of intrinsic mode functions (IMFs) at different characteristic time scales (or, equivalently, frequency scales). Comparisons of the evolutions of the instantaneous frequencies of the IMFs to the WT spectra of the time series, enables one to identify the dominant IMFs of the signals, as well as, the time scales at which the dominant dynamics evolve at different time windows of the responses; hence, it is possible to reconstruct complex transient responses as superpositions of the dominant IMFs involving different time scales of the dynamical response. Moreover, by superimposing the WT spectra and the instantaneous frequencies of the IMFs to the FEPs of the underlying hamiltonian system, one is able to clearly identify the multi-scaled transitions that occur in the transient damped dynamics, and to interpret them as 'jumps' between different branches of periodic orbits of the underlying hamiltonian system. As a result, this work develops a physics-based, multi-scaled framework and provides the necessary computational tools for multi-scaled analysis of complex multi-frequency transitions of essentially nonlinear dynamical systems.

Keywords: Multi-scaled analysis, nonlinear damped transitions, essential nonlinearity

1. Introduction

In this work we study complex nonlinear dynamic interactions between a linear dispersive rod and a strongly nonlinear end attachment. As such, this work is a continuation of previous works (Vakakis et al., 2004; Georgiadis et al., 2006) where elastic wave interactions and nonlinear resonance captures in systems of elastic continua with essentially nonlinear end attachments were analytically and computationally studied. New elements in the present analysis is the utilization of *frequency energy-plots (FEPs)* for depicting and *interpreting essentially nonlinear damped transitions in terms of the undamped dynamics*, and, additionally, application of *Hilbert-Huang transforms – HHTs* (Huang et al., 1998a; 2003) (also called *Empirical Mode Decomposition – EMD*) for decomposing the transient dynamics in terms of multi-scaled *intrinsic mode functions (IMFs)* that enable accurate multi-scaled identification and modeling of the dominant nonlinear resonant interactions that occur in the measured time series. By interpreting damped nonlinear transitions in the frequency-energy plot in terms of resonant interactions of the dominant IMFs of these transitions we aim to formulate a new integrated physics-based, multi-scale method for analyzing and modeling the strongly nonlinear, complex dynamical interactions occurring between elastic continua and nonlinear boundary attachments.

The HHT (or EMD analysis) extracts oscillating modulations or modes imbedded in a measured time series. The method applies to nonlinear as well as nonlinear transient responses *empirically identifies intrinsic oscillatory modes (the IMFs) in the time series, and categorizes them in terms of their characteristic time scales.* The IMFs have usually a physical interpretation but this need not always be the case. HHT has been applied to a diverse field of system identification applications, including nonlinear water waves (Huang, 1999), biomedical engineering (Huang et al., 1998b), climate modelling (Wu et al., 1999), and costal sea wave modelling (Veltcheva, 2002). It is interesting to note that although the HHT has been proven to be effective in identifying and modelling multi-frequency time series, until recently no rigorous theoretical framework of the method existed; Kerschen et al., (2006b, 2006c), provided proof that the dominant IMFs of the time series extracted by the HHT coincide with the slow flow responses of the corresponding dynamical system, thus providing a theoretical framework for formulating a rigorous nonlinear system identification methodology based on the HHT. A first application of the HHT to a problem involving strongly nonlinear resonant interactions was provided in (Georgiades et al., 2006), where the transient damped dynamics of a finite rod with an essentially nonlinear end attachement was decomposed by means of the HHT, and the dominant IMFs of the rod and attachment dynamics identified. This decomposition enabled the identification of the frequencies at which the dominant resonant interactions between the rod and the attachment occurred, giving rise to targeted energy transfer phenomena.

2. Frequency – Energy Plot (FEP) of the Periodic Orbits of the Hamiltonian System

We consider a finite, elastically supported (dispersive) linear rod clamped at its left end, and coupled to a light mass by means of an essentially nonlinear (nonlinearizable) stiffness at its other boundary; the small mass of the attachment is scaled by the small parameter ε, $0 < \varepsilon << 1$, whereas the viscous damping of the system is also assumed to be weak, of $O(\varepsilon)$. The nonlinear attachment will also be referred to as nonlinear energy sink (NES), since, if properly designed (Georgiades et al., 2006), may passively absorb and dissipate a significant portion of the vibration energy of the rod. Denoting by $v(t)$ and $u(x,t)$, the displacements of the nonlinear attachment and the rod at the point x, respectively, we derive

the following mathematical problem (governing equations of motion complemented by boundary and initial conditions) in normalized form,

$$\begin{aligned}
&\frac{\partial^2 u(x,t)}{\partial t^2}+\omega_0^2 u(x,t)+\varepsilon\lambda_1\frac{\partial u(x,t)}{\partial t}-\frac{\partial^2 u(x,t)}{\partial x^2}=0 \qquad 0\le x\le L\\
&u(0,t)=0,\ \frac{\partial u(L,t)}{\partial x}=-\varepsilon\ddot{v}(t)\\
&\varepsilon\ddot{v}(t)+\varepsilon\lambda_2\left[\dot{v}(t)-\frac{\partial u(L,t)}{\partial t}\right]+C\left[v(t)-u(L,t)\right]^3=0\\
&u(x,0)=r(x),\ \frac{\partial u(x,0)}{\partial t}=s(x)\\
&v(0)=v_0,\ \dot{v}(0)=\dot{v}_0
\end{aligned} \tag{1}$$

where $r(x), s(x)$ are the initial displacement and velocity distributions of the rod, λ_1, λ_2 are viscous damping coefficients, L the length of the rod, and C the coefficient of the stiffness nonlinearity of the attachment. We note that the attachment is coupled to the rod by an essentially nonlinear (e.g., nonlinearizable) stiffness, and that the frequency ω_0 (the nondimensional distributed elastic support of the rod) represents the cut-off frequency of the uncoupled dispersive rod, e.g., the bounding frequency that separates its attenuation and propagation zones.

As a first step, *we wish to provide an interpretation of the transient damped dynamics in terms of the time-periodic orbits of the corresponding undamped (hamiltonian) system*. Hence, we consider the corresponding undamped mathematical problem by setting $\lambda_1=0, \lambda_2=0$ in equations (1):

$$\begin{aligned}
&\frac{\partial^2 u(x,t)}{\partial t^2}+\omega_0^2 u(x,t)-\frac{\partial^2 u(x,t)}{\partial x^2}=0 \qquad 0\le x\le L\\
&u(0,t)=0,\quad \frac{\partial u(L,t)}{\partial x}=-\varepsilon\ddot{v}(t)\\
&\varepsilon\ddot{v}(t)+C\left[v(t)-u(L,t)\right]^3=0
\end{aligned} \tag{2}$$

Initial conditions are omitted from (2) since the problem of computing the undamped periodic orbits is a nonlinear boundary value problem (NLBVP), in contrast to the damped problem (1) which is formulated as a Cauchy (initial value) problem.

To compute the T-periodic solutions of system (1), we express the displacements in the following series forms,

$$\begin{aligned}
u(x,t)&=\sum_{k=1}^{\infty} C_k(x)\cos\left[(2k-1)\Omega t\right]+\sum_{k=1}^{\infty} S_k(x)\sin\left[(2k-1)\Omega t\right]\\
v(t)&=\sum_{k=1}^{\infty} V_{c,k}\cos\left[(2k-1)\Omega t\right]+\sum_{k=1}^{\infty} V_{s,k}\sin\left[(2k-1)\Omega t\right]
\end{aligned} \tag{3}$$

where by $\Omega=2\pi/T$ denotes the basic frequency of the periodic motion. Substituting (3) into the partial differential equation in (2) and taking into account the imposed boundary conditions, we obtain the following series of linear boundary value problems (BVPs) governing the spatial distributions $C_k(x)$ and $S_k(x)$, $k=1,2,\ldots$:

$$\frac{d^2C_k(x)}{dx^2}+\left[\left(2k-1\right)^2\Omega^2-\omega_0^2\right]C_k(x)=0$$
$$\frac{d^2S_k(x)}{dx^2}+\left[\left(2k-1\right)^2\Omega^2-\omega_0^2\right]S_k(x)=0 \tag{4}$$
$$C_k(0)=S_k(0)=0,\ \frac{dC_k(L)}{dx}=\varepsilon\left(2k-1\right)^2\Omega^2V_{c,k},\ \frac{dS_k(L)}{dx}=\varepsilon\left(2k-1\right)^2\Omega^2V_{s,k}$$

The solutions of these problems are expressed as,

$$C_k(x)=\hat{C}_k\sin\left[x\sqrt{\left(2k-1\right)^2\Omega^2-\omega_0^2}\right]$$
$$S_k(x)=\hat{S}_k\sin\left[x\sqrt{\left(2k-1\right)^2\Omega^2-\omega_0^2}\right] \tag{5a}$$

where,

$$\hat{C}_k=\frac{\varepsilon\left(2k-1\right)^2\Omega^2V_{c,k}}{\cos\left[L\sqrt{\left[\left(2k-1\right)^2\Omega^2-\omega_0^2\right]}\right]\sqrt{\left[\left(2k-1\right)^2\Omega^2-\omega_0^2\right]}} \tag{5b}$$

and,

$$\hat{S}_k=\frac{\varepsilon\left(2k-1\right)^2\Omega^2V_{s,k}}{\cos\left[L\sqrt{\left[\left(2k-1\right)^2\Omega^2-\omega_0^2\right]}\right]\sqrt{\left[\left(2k-1\right)^2\Omega^2-\omega_0^2\right]}} \tag{5c}$$

We note at this point that expressions (5a-c) are valid in the entire range of frequencies $\Omega\in\left[0,\infty\right)$, e.g., for harmonics with frequencies in both the propagation and attenuation zones of the uncoupled linear rod. Indeed, for values of Ω for which $\left(2k-1\right)^2\Omega^2-\omega_0^2<0$ for some $k\in N^+$, the following well-known relations are employed, $\sin(j\alpha)=j\sinh(\alpha),\ \cos(j\alpha)=\cosh(\alpha)$ with $j=\sqrt{-1}$, rendering expressions (5a) real quantities, with attenuating spatial envelopes.

Expressions (5a-c) are derived in terms of the amplitudes $V_{s,k}$ and $V_{c,k}$ of the harmonics of the nonlinear attachment. These are computed by substituting (3) and (5a-c) into the nonlinear ordinary differential equation in (2), leading to the following algebraic expression containing infinite series with index k:

$$-\varepsilon\left\{\sum_{k=1}^{\infty}\left(2k-1\right)^2\Omega^2\left(\ V_{c,k}\cos\left[\left(2k-1\right)\Omega t\right]+V_{s,k}\sin\left[\left(2k-1\right)\Omega t\right]\ \right)\right\}+$$
$$C\left\{\ \sum_{k=1}^{\infty}\left(1-\varepsilon\left(2k-1\right)^2\Omega^2\left[\left(2k-1\right)^2\Omega^2-\omega_0^2\right]^{-1/2}\tan\left(L\sqrt{\left(2k-1\right)^2\Omega^2-\omega_0^2}\right)\right)\times \tag{6}$$
$$\left(V_{c,k}\cos\left[\left(2k-1\right)\Omega t\right]+V_{s,k}\sin\left[\left(2k-1\right)\Omega t\right]\right)\ \right\}^3=0$$

Expanding the power in (6), and setting the coefficients of the trigonometric functions $\cos\left[\left(2k-1\right)\Omega t\right],\ \sin\left[\left(2k-1\right)\Omega t\right],\ k=1,2,...$ separately equal to zero, one derives an infinite set of nonlinear algebraic equations for the coefficients $V_{c,k}$ and $V_{s,k}$ that determine the periodic solutions of the hamiltonian system. For numerical reasons, this infinite set was truncated by considering terms only up to the fifth harmonic (e.g., $k=1,2,3$), and omitting higher harmonics. The resulting truncated set of six nonlinear algebraic equations is then

numerically solved for the amplitudes $V_{s,k}$ and $V_{c,k}$, which also determine approximately the periodic motion of the system through relations (3) and (5).

In Figure 1 the relative displacement $[v(t)-u(L,t)]$ of the truncated system (e.g., the periodic solutions of the hamiltonian system) are depicted for parameters $\varepsilon = 0.05$, $\omega_0 = 1.0$, $C = 1.0$, $L = 1.0$ and $\lambda_1 = \lambda_2 = 0$ in a frequency – energy plot (FEP); only the frequency range covering the two leading modes of the uncoupled linear rod is considered. The FEP depicts the logarithm of the energy of a given periodic orbit, $Log_{10}(E)$, versus the fundamental frequency Ω (in rad/sec) of the same orbit. The (conserved) energy E of the periodic orbit is computed by the following expression:

$$E = \frac{1}{2}\int_0^L \left[\frac{\partial u(x,t)}{\partial t}\right]^2 dx + \frac{1}{2}\int_0^L \left[\frac{\partial u(x,t)}{\partial x}\right]^2 dx + \frac{1}{2}\omega_0^2 \int_0^L u^2(x,t)\,dx + \frac{1}{2}\varepsilon v^2(t) + \frac{1}{4}C\left[v(t)-u(L,t)\right]^4 \tag{7}$$

(Figure 1)

Considering the FEP, one discerns the existence of two low-frequency asymptotes corresponding to the two leading modes of the linear uncoupled rod:

$$\omega_n = \sqrt{\omega_0^2 + \frac{(2n-1)^2\pi^2}{4L^2}}, \quad n = 1,2 \quad \text{(Low-energy asymptotes)} \tag{8}$$

For the parameters used for computing the FEP one computes $\omega_1 = 1.8621\, rad/\sec$ and $\omega_2 = 4.8173\, rad/\sec$. In addition, there exist two high-frequency asymptotes. Noting that at high energies and finite frequencies the essentially nonlinear stiffness of system (2) behaves as a massless rigid link, the high-frequency asymptotes are computed as the eigenfrequencies of the following alternative limiting linear system,

$$\frac{\partial^2 u(x,t)}{\partial t^2} + \omega_0^2 u(x,t) - \frac{\partial^2 u(x,t)}{\partial x^2} = 0, \quad 0 \le x \le L$$
$$u(0,t) = 0, \quad \frac{\partial u(L,t)}{\partial x} = -\varepsilon \frac{\partial^2 u(L,t)}{\partial t^2} \tag{9}$$

e.g., the dispersive rod with a mass ε attached to its right end. The eigenfrequencies of this limiting system are computed by solving the following transcendental equation:

$$\tan\left[L\sqrt{\hat{\omega}^2 - \omega_0^2}\right] = \frac{\sqrt{\hat{\omega}^2 - \omega_0^2}}{\varepsilon \hat{\omega}^2} \quad \text{(High-energy asymptotes)} \tag{10}$$

For the parameters corresponding to the FEP of Figure 1 one computes the two leading high-energy asymptotes as, $\hat{\omega}_1 = 1.7728\, rad/\sec$ and $\hat{\omega}_2 = 4.5916\, rad/\sec$.

Since the principal aim for constructing the FEP is to interpret the (weakly) damped dynamics of system (1), it is necessary to discuss the structure of the various branches of periodic orbits of the underlying hamiltonian system (2), and to distinguish between the dynamical responses that occur at different frequency and energy ranges. The FEP of Figure 1 possesses two types of branches of periodic motions, namely *backbone (global) branches* and *subharmonic tongues (local branches).* Backbone branches consist of nearly monochromatic periodic solutions possessing a dominant harmonic component and higher harmonics at integer multiples of the dominant harmonic. These branches are defined over extended frequency and energy ranges, and are composed of periodic solutions that are mainly localized at the nonlinear attachment, except in neighborhoods of the linearized eigenfrequencies of the rod, $\omega_1, \omega_2, \ldots$ (where the spatial distributions of the periodic motions resemble those of the corresponding rod mode shapes and are localized at the rod), and in

neighborhoods of the high-energy asymptotes $\hat{\omega}_1, \hat{\omega}_2, \ldots$ (where the relative motions between the nonlinear attachment and the rod end tend to zero). In Figure 2 representative periodic motions lying on backbone branches of the system are depicted. These can be considered as *analytically predicted* periodic solutions of the system, since their initial conditions are determined by solving the truncated system (6). To check the correctness of the analytical results, comparisons were made with direct numerical simulations of the dynamics based on a finite element (FE) model for the rod (to be described in the next section); these comparisons proved that the analytically predicted branches of periodic orbits were indeed accurate, and, hence, validated the analytical formulation and the FEP of Figure 1.

(Figures 2,3)

A different set of periodic solutions lie on *subharmonic tongues (local branches);* these are multi-frequency periodic motions, with frequencies being approximately equal to rational multiples of the eigenfrequencies ω_n of the uncoupled rod. Each tongue is defined over a finite energy range, and is composed of two distinct branches of subharmonic solutions; at a critical energy level the two branches coalesce in a bifurcation that signifies the end of that particular tongue and the elimination of the corresponding subharmonic motions at higher energy values. It can be proven that there exists a countable infinity of tonques emanating from the backbone branches at frequencies in rational relation to the eigenfrequencies of the uncoupled linear rod ω_n. It follows that subharmonic motions on the tongues possess dominant harmonics that are integrably related to certain eigenfrequencies of the uncoupled rod. On a given tongue the responses of any point the rod and of the attachment resemble those of two linear oscillators, albeit possessing different (but integrably related) eigenfrequencies. *Hence, the interesting (and paradoxical) observation can be drawn, namely, that on the essentially nonlinear tongues* (they are characterized as such since they exist due to the essential stiffness nonlinearity) *the rod-attachment system behaves nearly as an equivalent two-frequency linear system*.

In the FEP of Figure 1, only a subset of leading tongues are depicted; for example, the tongue depicted in Region I (Fig. 1b) is in the vicinity of $\omega_4/3$, so that, in subharmonic motions on this tongue the response of the nonlinear attachment possesses a dominant harmonic with frequency $\omega_4/3$ (and a minor harmonic at ω_4), whereas the response of the rod end possesses a dominant harmonic at ω_4 (and a minor harmonic at $\omega_4/3$). In what follows a tongue labeled $T_{p/q}^{(n)}$ denotes the branch of subharmonic motions where the frequency of the dominant harmonic component of the nonlinear attachment is nearly equal to $(p/q)\omega_n$, whereas that of the rod end is equal to ω_n; it follows that the relative displacement $[v(t)-u(L,t)]$ for subharmonic motion on tongue $T_{p/q}^{(n)}$, is signified by two main harmonics at frequencies ω_n and $(p/q)\omega_n$. Using this notation, the subharmonic tongue depicted in Figure 1b is labeled as $T_{1/3}^{(4)}$. In Figure 3 three subharmonic orbits on the tongue $T_{1/3}^{(4)}$ of the FEP are depicted in the neighborhood of $\omega_4/3$. Again, comparisons to direct FE simulations of the dynamics were made, which proved the correctness of the analytically predicted subharmonic motions.

In the next section the damped responses of system (1) are studied in detail. By wavelet transforming the measured time series of the attachment and the rod end and superimposing the resulting wavelet spectra to the FEP, one may discern a direct link between the damped and undamped dynamics. This enables one to classify and understand the nonlinear transitions that occur in the damped dynamics as the energy (and frequency) of the response

decreases. Further analysis of the damped dynamics is performed by post processing the time series by the Hilbert Huang Tranform (HHT).

3. Study of Multi-scaled Transitions in the Damped Dynamics

The study of the damped dynamics of system (1) was performed through direct simulations of the equations (1) and post processing of the transient results. The responses of the rod-attachment system were computed by the finite elements method (FEM). For these computations the rod was discretized in 200 finite elements, which ensured a five-digit convergence of the computations of the three leading modes of the rod. Regarding the numerical integrations of the equations of motion (1), the Newmark algorithm was utilized with parameters chosen to ensure unconditional stability of the numerical algorithm. Finally, the sampling frequency was such that the eigenfrequencies of the leading three modes of the rod are less than 6% of the sampling frequency. Regarding viscous dissipation, proportional damping in the rod was assumed, by expressing the damping matrix as, $\mathbf{D} = a_1\mathbf{M} + a_2\mathbf{K}$, where **M** and **K** are the mass and stiffness matrices of the rod. The parameters used for the FEM computations were chosen as $\varepsilon = 0.05$, $C = 1.0$, $L = 1.0$, $\omega_0 = 1.0$, $\lambda_2 = 0.2$, $\alpha_1 = 0.001$, and $\alpha_2 = 0.0$, and the damped response is initiated for different sets of initial conditions of the rod and the nonlinear attachment.

The resulting damped transient responses of the system are post processed by applying two different algorithms, namely, numerical wavelet transforms (WTs) and Hilbert Huang Transforms (HHTs). First, the time series are analyzed by employing a Matlab-based Morlet WT algorithm developed at Université de Liège by Dr.V.Lenaerts in collaboration with Dr.P.Argoul from the 'Ecole Nationale des Ponts et Chaussees' [for recent works of this group see (Argoul and Le, 2003) and (Le and Argoul, 2004)]. As output of this analysis one computed WT contour plots (WT spectra) depicting the amplitudes of the WT of the analyzed signals as functions of frequency and time; heavy shaded areas correspond to regions where the amplitude of the WT is high, whereas lightly shaded ones correspond to low amplitudes of the WT. These plots enable one to deduce the temporal evolutions of the dominant frequency components of the signals analyzed, as well as, transitions between different modes that participate in the transient nonlinear responses (Lee et al., 2005; Kerschen et al., 2006a).

Further analysis of the numerical time series was performed by applying the Hilbert Huang Transform (HHT). This is a method to decompose a signal (time series) in terms components called *Intrinsic Mode Functions (IMFs)* satisfying the following three main *ad hoc* conditions:

- For the duration of the entire time series, the number of extrema and of zero crossings of each IMF should either be equal or differ at most by one
- At any given time instant, the mean value (moving average) of the local envelopes of the IMFs defined by their local maxima and minima should be zero
- The superposition of all IMFs should reconstructs the time series

Hence, this extracts oscillating modulations or modes imbedded in the data. In essence, one *empirically identifies intrinsic oscillatory modes in the damped time series, and categorizes them in terms of their characteristic time scales, by considering the successive extreme values of the signal.* The IMFs have usually a physical interpretation as far as their characteristic scales are concerned (indeed, as shown below, certain IMFs possess instantaneous frequencies that are nearly identical to resonance frequencies of the rod or the nonlinear attachment); but this need not always be the case. This implies that certain IMFs may represent artificial (non-physical) oscillating modes of the data. In an additional step,

Hilbert – transform of the IMFs is performed to compute the temporal evolutions of their instantaneous amplitudes and frequencies, which, in turn, can be used for the construction of the Hilbert spectra of the time series. In this work the HHT was implemented in Matlab.

The HHT combined with the WT enables one to determine the *dominant IMFs* in the damped time series. This is achieved by superimposing the plots of instantaneous frequencies of the IMFs to the corresponding wavelet spectra of the time series; clearly, the instantaneous frequencies of the dominant IMFs should coincide with the main harmonic components of the corresponding wavelet spectra in the time windows where they are dominant. It follows, that by combining WTs and HHTs one is able to determine the main dominant oscillating components in the measured time series and, hence, to perform order reduction and low-order modelling of the measured transient signals. This process provides also the characteristic time scales where the dominant nonlinear dynamics of the rod-attachment interaction take place. Moreover, by adopting this analysis one can identify and analyze the most important nonlinear resonance interactions between the rod and the attachment, that are responsible for the nonlinear energy exchanges between these two subsystems. Hence, as shown below, by studying the resonance interactions between dominant IMFs of the attachment and the rod responses, one can gain insight into the complex resonant dynamics that govern passive broadband energy exchanges between the rod to the attachment. To better study such exchanges, in the following numerical simulations the energy transaction history for each simulation has been computed, with positive values denoting energy transfer from rod to attachment, and negative values indicating reverse energy flow.

In what follows the damped transitions of system (1) resulting from different sets of initial conditions will be analyzed. First, initial conditions corresponding to point A on the main backbone branch of the FEP are considered, at frequency $\omega = 0.6\, rad/s$ (cf. Figure 1). The initial conditions for the rod and the nonlinear attachment are approximately computed using the method of section 2 as follows,

$$\begin{aligned} v(0) &\approx \left\{ V_{c,1}\cos(\omega t) + V_{c,2}\cos(3\omega t) + V_{c,3}\cos(5\omega t) \right\}_{t=0} \Rightarrow\ v(0) \approx -0.1650 \\ u(x,0) &\approx \left\{ \hat{C}_1 \sin\left(x\sqrt{\omega^2 - \omega_0^2}\right)\cos(\omega t) + \hat{C}_2 \sin\left(x\sqrt{9\omega^2 - \omega_0^2}\right)\cos(3\omega t) + \right. \\ &\left. \hat{C}_3 \sin\left(x\sqrt{\left[25\omega^2 - \omega_0^2\right]}\right)\cos(5\omega t) \right\}_{t=0} \Rightarrow\ u(0,0) \approx -0.0052 \end{aligned} \tag{11}$$

with , $V_{c1} = -0.1597,\ V_{c2} = -0.0054,\ V_{c3} = 0.0001$, $\hat{C}_1 = 0.0027$, $\hat{C}_2 = -0.0079$, and $\hat{C}_3 = -0.00002$. In the undamped system these initial conditions correspond to a periodic motion which is predominantly localized to the nonlinear attachment. In Figure 4 the damped responses of the attachment and the point of connection of the rod are depicted, together with the depiction of the wavelet spectrum of the damped relative motion $\left[v(t) - u(L,t)\right]$ superimposed on the FEP of the hamiltonian system. It is observed that as energy decreases due to damping dissipation the motion makes a transition following closely the main backbone branch of the corresponding hamiltonian system; this observation confirms that for sufficiently weak damping the damped response is dominated by the dynamics of the underlying hamiltonian system. The nonlinear dynamic interaction between the rod and the attachment is now examined in more detail.

The transient energy transaction history between the rod and the nonlinear attachment is depicted in Figure 5. Positive spikes indicate energy transmission from the rod to the attachment, whereas negative spikes indicate energy backscattered from the attachment back to the rod. The energy transaction history of Figure 5 indicates the presence of (weak) nonlinear beat phenomena between the two subsystems, with continuous energy being

exchanged between them; it is noted that in the damped transition of Figure 4 the motion is predominantly localized in the nonlinear attachment throughout the motion, so that only weak energy exchanges occurring between the two subsystems. As shown in (Georgiades et al., 2006) for different sets of initial conditions stronger energy exchanges may occur, resulting in vigorous targeted energy transfers from the rod to the nonlinear attachment; these transfers may be realized either through nonlinear beats, through one-way energy transfers from the rod to the attachment (evidenced represented by a series of only positive spikes in the energy transaction diagram), or through a combination of both.

(Figures 4,5)

In Figure 6 the results of the Hilbert-Huang Transformations (HHTs) of the damped responses of the nonlinear attachment and the rod end are depicted. The three leading IMFs of the damped responses are presented, and in Figure 7 IMF-based reconstructions of the same damped responses are shown. It is shown that the transient response of the nonlinear attachment is approximately reconstructed using only its first and second IMFs, whereas the response of the rod end is approximated by only its first IMF; given the relation between the leading IMFs and the reduced slow-flow dynamics of the rod-attachment system (Kerschen et al., 2006b), the results presented in Figure 7 imply that the transient nonlinear dynamics of Figure 4 can be approximated by low-dimensional reduced-order models.

(Figures 6,7)

An interesting series of nonlinear transitions is depicted in the second numerical simulation of the damped dynamics depicted in Figure 8, corresponding to initial conditions at point B on the subharmonic tongue $T_{1/5}^{(4)}$ of the FEP (e.g., an undamped subharmonic orbit with dominant frequencies $\omega = 2.214\, rad/s \approx \omega_4/5$ and ω_4 – cf. Figure 1). The existence of transitions is evidenced by the irregular amplitude modulations of the time series (especially the one corresponding to the nonlinear attachment), or equivalently, by their multi-frequency content. A better representation of the transitions in the damped dynamics is achieved by superimposing the wavelet spectrum of the relative motion $[v(t)-u(0,t)]$ to the FEP of the undamped system (cf. Figure 8b); the following transitions are then discerned:

I. Initial high energy transition from the subharmonic tongue $T_{1/5}^{(4)}$ to tongue $T_{2/3}^{(1)}$ (note the appearance of two dominant harmonics at frequencies ω_4 and $\omega_4/5$ during this Stage at the FEP of Figure 8c).

II. Subharmonic capture on $T_{2/3}^{(1)}$ with the nonlinear attachment possessing a nearly constant dominant harmonic component of frequency $2\omega_1/3$ (but also a minor harmonic of frequency ω_1)

III. Transition from tongue $T_{2/3}^{(1)}$ to tongue $T_{1/3}^{(1)}$ and subharmonic capture on $T_{1/3}^{(1)}$ (signified by a strong harmonic at frequency $\omega_1/3$ and a weaker harmonic at frequency ω_1)

IV. Final low-energy transition to a linearized state, where the response of the nonlinear attachment approaches zero and the dynamics is dominated by the response of the linear rod (where the motion is nearly confined)

These complex transitions are due to the fact that the essentially nonlinear attachment lacks a preferential frequency of oscillation (since it possesses zero linearized stiffness), which enables it to engage in fundamental or subharmonic resonance captures (Lee et al., 2005; Kerschen et al., 2006a) with different modes of the linear rod, at arbitrary frequency ranges; equivalently, the essential stiffness nonlinearity of the attachment leads to a series of resonance capture cascades with the rod. As discussed in (Kerschen et al., 2006a) such

resonance capture cascades may lead to strong targeted energy transfer phenomena from the rod to the attachment, which then acts, in essence, as *nonlinear energy sink* [for a detailed study of these targeted energy transfers in the system under consideration the reader is referred to (Georgiades et al., 2006)].

(Figure 8)

The damped transitions depicted in Figure 8 are now analyzed in detail by HHT. The stages outlined above will be examined separately, with the aim to model the dynamics and to determine the time scales of the nonlinear interaction between the rod and the nonlinear attachment (or NES). Starting with the initial high-energy transition from tongue $T_{1/5}^{(4)}$ to tongue $T_{2/3}^{(1)}$ (Stage 1, $0 < t < 160\,s$), HHT analysis indicates that the NES response is dominated by its 1st IMF (cf. Figure 9), whereas, the rod end response is approximately modeled by two dominant IMFs, namely, its 1st and 2nd IMFs (cf. Figure 10). Indeed, noticing that the instantaneous frequencies of the aforementioned dominant IMFs coincide with dominant harmonic components of the corresponding transient responses, one concludes that the nonlinear dynamics of the rod-NES transient interaction is low-dimensional, with the dynamics of the NES resembling the response of a single-DOF oscillator with frequency approximately $\omega_4 / 5 \approx 2.214\,rad/\mathrm{s}$, whereas the dynamics of the rod end resembling the superposition of two single-DOF oscillators with frequencies ω_4 and $\omega_4 / 5$, respectively. Moreover, the 1st IMF of the NES is in near 1:5 resonance with 1st IMFof the rod end, and in near 1:1 resonance with 2nd IMF of the rod end. Hence, HHT analysis indicates there is one dominant time scale in the transient dynamics of the NES and two dominant time scales in the dynamics of the rod end. These results are confirmed by the time series reconstructions depicted in Figures 9b and 10b, which prove the low-dimensionality of the NES – rod end nonlinear interaction during this initial (and high energy) stage of the motion.

(Figures 9,10)

Proceeding now to the more complicated damped transition occurring in Stage II ($160 < t < 420\,s$) where the dynamics is captured at tongue $T_{2/3}^{(1)}$, the NES response appears to be dominated (and modeled) by its leading two IMFs (cf. Figure 11), which indicates that in this case the NES responds like a two-DOF oscillator. Considering the rod end response, one establishes the existence of three dominant IMFs (the leading three IMFs depicted in Figure 12), with the instantaneous frequency of the 1st IMF appearing to undergo modulated oscillations, and that of the 2nd IMF to suffer sudden transitions (jumps) with increasing time. This type of complex behavior of the IMFs is distinctly different from that observed in Stage I and is characteristic of *intrawaves* in the time series (Huang et al., 1998a). This means that a dominant harmonic component of an oscillatory mode (IMF) of the response possesses a frequency that oscillates about a constant value. The existence of intrawaves in oscillatory modes (IMFs) is one of the nonlinear effects detected in typical nonlinear systems, such as the forced Duffing oscillator, the Lorenz system, and the Rossler chaotic attractor where the wavelet spectra couldn't detect them; as mentioned in (Huang et al., 1998a), '…in fact such an instantaneous frequency presentation actually reveals more details of the system: it reveals the variation of the frequency within one period, a view never seen before…' The time series reconstructions depicted in Figures 11b and 12b confirm that the superpositions of the dominant IMFs accurately model the damped transition during this Stage of the motion. Note that the higher dimensionality of the NES and rod end responses observed in this case, signifies that the complexity of the dynamics increases compared to Stage I.

Considering the resonance interactions between the IMFs of the NES and the rod end responses during Stage II of the damped response, the 1st IMF of the NES is in near 2:3 internal resonance with the 2nd IMF of the rod end in the time interval $160 < t < 250\,s$, and

with the 3rd IMF of the rod end in the interval $250 < t < 350\,s$; moreover, there appears to be 1:1 internal resonance between the 1st IMF of the NES and the 3rd IMF of the rod end in the time interval $160 < t < 250\,s$. The transition of the dynamics from tongue $T_{2/3}^{(1)}$ to tongue $T_{1/3}^{(1)}$ is signified by the decrease of the instantaneous frequency of the 1st IMF of the NES in the interval $t > 350\,s$. The 1st IMF of the rod end possesses an oscillatory instantaneous frequency about ω_4 in the interval $160 < t < 300\,s$, and about ω_3 and ω_4 in the interval $300 < t < 420\,s$ (due to intrawaves, as discussed above); this result of the HHT agrees qualitatively with the late excitation of the 3rd linear mode of the rod, as indicated by the wavelet transform of the signal. The 2nd IMF of the rod end possesses an instantaneous frequency which is approximately equal to ω_1 for $160 < t < 250\,s$, and is oscillatory about ω_2 for $250 < t < 350\,s$; this, when the wavelet transform of the time series of the rod end response does not indicate any excitation of the second mode of the rod at Stage II (which demonstrates the clear advantages of the HHT in analyzing complex signals compared to the wavelet transform).

(Figures 11,12)

In Figures 13-15 the results of the HHT analysis of Stages III and IV ($t > 420\,s$) are depicted. In this case the NES response possesses three dominant IMFs, whereas that of the rod end four. The resonance capture of the dynamics on tongue $T_{1/3}^{(1)}$ is signified by the fact that the instantaneous frequency of the 1st IMF of the NES response is approximately equal to $\omega_1/3$ in the time interval $420 < t < 820\,s$ (with the exception of a 'high frequency burst' in the neighborhood of $t = 500\,s$), whereas, the transition from $T_{1/3}^{(1)}$ to the linearized regime is signified by the decrease of the instantaneous frequency of the same IMF for $t > 820\,s$. It is interesting to note that in the time interval where the 'high frequency burst' of the 1st IMF of the NES occurs, the 2nd IMF of the NES 'locks' to the value $\omega_1/3$, and, hence, through superposition provides the necessary correction in the reconstruction of the overall time series in that time interval. Moreover, by studying the waveform of the 3rd IMF of the NES one notes that this IMF dominates the transition from $T_{1/3}^{(1)}$ to the linearized regime occurring for $t > 800\,s$. Considering the IMFs of the rod end response, one notes intrawave effects centered at the linearized eigenfrequencies of the rod, $\omega_1,...,\omega_4$, similarly to what was observed in the HHT results of the response in Stage II.

(Figures 13,14,15)

The presented results demonstrate the usefulness of the HHT as a computational tool for postprocessing nonlinear dynamics that involve multiple resonance captures and escapes. In fact, the previous results indicate that the HHT can capture delicate features of the dynamics (such as intrawave effects or excitation of modes) that are not evident in the corresponding wavelet transforms. Nevertheless, the presented computational analysis shows that the combination of HHT and wavelet analysis forms a powerful computational methodology for postprocessing and modeling of complex nonlinear transient responses of practical structural systems.

4. Concluding Remarks

The analysis of complex, multi-frequency nonlinear transitions in the damped dynamics of a viscously damped dispersive finite rod coupled to an essentially nonlinear oscillator was considered. It was shown that for weak damping, a clear understanding of dynamical transitions in this system can be gained by wavelet transforming the time series and

superimposing the resulting wavelet spectra in the frequency – energy plot (FEP) of the periodic orbits of the underlying hamiltonian system. This should not be surprising, given that the effect of weak damping in the response can be considered to be parasitic, e.g., it is not expected to give rise to any new dynamical phenomena; as a result, as energy decreases with time the weakly damped nonlinear dynamics either follow damped manifolds close to manifolds of periodic orbits of the hamiltonian system, or suffer sudden transitions (jumps) between different branches of solutions. These transitions can be clearly represented in the FEP.

The damped responses of the system were initially analyzed by the numerical Morlet Wavelet Transform (WT), and then by the Empirical Mode Decomposition (EMD) or Hilbert-Huang Transform (HTT), whereby, the time series are decomposed in terms of intrinsic mode functions (IMFs) at different characteristic time scales (or, equivalently, frequency scales). It was shown that the HHT is capable of analyzing even complex nonlinear transitions, by providing the dominant frequency components (or equivalently, time scales) were the nonlinear phenomena take place. In addition, the HHT can detect delicate features of the dynamics, such as intrawaves – e.g., IMFs with modulated instantaneous frequencies, that the wavelet transform cannot. More importantly, due to the HHT algorithm, the superposition of the dominant IMFs of the signal reconstructs the signal itself, and, hence, these dominant IMFs may be interpreted as outputs of intrinsic modal oscillators. It follows, that the determination of the dominant IMFs of a complex nonlinear signal, paves the way for modeling this signal, for determining the dimensionality of its dynamics, and for ultimately performing multi-scaled system identification of the underlying dynamics of the system.

Acknowledgments

This work was supported in part by a grant for basic research ‘HRAKLEITOS’ co-funded by the European Commission and the General Secretariat for Research and Technology of the Hellenic Ministry of Development; and by AFOSR grant FA9550-04-1-0073.

References

Argoul P., Le T.P., 2003. Instantaneous Indicators of Structural Behaviour Based on the Continuous Cauchy Wavelet Analysis, Mechanical Systems and Signal Processing, Vol. 17, No.1, pp. 243-250.

Georgiades F., Vakakis A.F., and Kerschen G., 2006. Broadband Passive Targeted Energy Pumping from a Linear Dispersive Rod to a Lightweight Essentially Nonlinear End Attachment, International Journal for Nonlinear Mechanics (in press).

Huang N.E., Z. Shen, S.R. Long, M.C. Wu, H.H. Shih, Q. Zheng, N.C. Yen, C.C. Tung, H.H. Liu, 1998a. The Empirical Mode Decomposition and the Hilbert Spectrum for Nonlinear and Non-stationary Time Series Analysis, Proceedings of the Royal Society of London, Series A, Vol. 454, pp. 903-995.

Huang W., Shen Z., Huang N.E., Fung Y.C., 1998b. Engineering Analysis of Biological Variables: An Example of Blood Pressure Over 1 Day, Proceedings of the National Academy of Sciences, Vol. 95, pp. 4816-4821.

Huang N.E., Shen Z., Long S.R., 1999. A New View of Nonlinear Water Waves: The Hilbert Spectrum, Annual Review of Fluid Mechanics, Vol. 31, pp. 417-457.

Huang N.E., , M.C. Wu, S.R. Long, S.S.P. Shen, W. Qu, P. Gloersen, K.L. Fan, 2003. A Confidence Limit for the Empirical Mode Decomposition and Hilbert Spectral Analysis, Proceedings of the Royal Society of London, Series A, Vol. 459, pp. 2317-2345.

Kerschen G., Y. Sup Lee, A.F. Vakakis, D.M. McFarland, L.A. Bergman, 2006a. Irreversible Passive Energy Transfer in Coupled Oscillators with Essential Nonlinearity, SIAM Journal on Applied Mathematics, Vol. 66, No.2, pp. 648-679.

Kerschen, G., Vakakis, A.F., Lee, Y.S., McFarland, D.M. and Bergman, L.A., 2006b. 'Toward a Fundamental Understanding of the Hilbert-Huang Transform in Nonlinear Structural Dynamics,' Proceedings of the 24th International Modal Analysis Conference (IMAC), St-Louis, MO.

Kerschen, G., Vakakis A.F., Lee Y.S., McFarland D.M., Bergman L.A., 2006c. 'Toward a Fundamental Understanding of the Hilbert-Huang Transform in Nonlinear Structural Dynamics,' Journal of Vibration and Control (submitted).

Le T.-P., Argoul P., 2004. Continuous Wavelet Tranform for Modal Identification Using Free Decay Response, Journal of Sound and Vibration, Vol. 277, pp. 73-100.

Lee Y.S., Kerschen G., Vakakis A.F., Panagopoulos P.N., Bergman L.A., McFarland D.M., Complicated Dynamics of a Linear Oscillator with a Light, Essentially Nonlinear Attachment 2005. Physica D Vol. 204, No. 1-2, pp. 41-69.

Vakakis A.F., L.I. Manevitch, A. Musienko, G. Kerschen, L.A. Bergman, 2004. Transient Dynamics of a Dispersive Elastic Wave Guide Weakly Coupled to an Essentially Nonlinear End Attachment. Wave Motion, Vol. 41/2, pp. 109-132.

Veltcheva A.D., 2002. Wave and Group Transformation by a Hilbert Spectrum, Coastal Engineering Journal, Vol. 44, No. 4, pp. 283-300.

Wu M.L., Schubert S., Huang N.E., 1999. The Development of the South Asian Summer Monsoon and the Intraseasonal Oscillation, Journal of Climate, Vol. 12, pp. 2054-2075.

Figure Captions

1. FEP of the hamiltonian system: (a) Backbone branches of periodic motions and tongues of subharmonic motions; (b,c) Details of regions I and II; numbers (▼) correspond to the periodic orbits depicted in Figures 2 and 3, and letters (●) to the numerical simulations of section 3.
2. Periodic orbits on backbone branches of the FEP: (1) $\omega = 0.6\,rad/\sec$, (2) $\omega = 1.3\,rad/\sec$, (3) $\omega = 1.75\,rad/\sec$, (4) $\omega = 2.3\,rad/\sec$, (5) $\omega = 4.5\,rad/\sec$, (6) $\omega = 1.87\,rad/\sec$, (7) $\omega = 4.83\,rad/\sec$; ——— Rod end, - - - - - - Nonlinear attachment.
3. Subharmonic periodic orbits on the subharmonic tongue $T_{1/3}^{(4)}$ (region I of the FEP): (8) $\omega = 3.72\,rad/\sec,\ Log(Energy) = 0.645$, (9) $\omega = 3.72\,rad/\sec,\ Log(Energy) = 1.015$, (10) $\omega = 3.72\,rad/\sec,\ Log(Energy) = 0.48$; ——— Rod end, - - - - - - Nonlinear Attachment.
4. Damped response initiated at point A of the FEP of Figure 1: (a) Transient responses $v(t)$ and $u(x,t)$; (b) Wavelet spectrum of the relative response $[v(t)-u(L,t)]$ superimposed to the FEP of the hamiltonian system.
5. History of energy transaction between the rod and the nonlinear attachment for the damped responses of Figure 4.
6. Leading IMFs of the nonlinear attachment and the rod end for the damped responses of Figure 4.
7. Time series reconstructions of the damped responses of Figure 4 taking into account the leading two IMFs of the response of the nonlinear attachment, and the leading IMF of the rod end response.
8. Damped response initiated at point B of the FEP of Figure 1: (a) Transient responses $v(t)$ and $u(L,t)$; (b) History of energy transaction between the rod and the nonlinear attachment; (c) Wavelet spectrum of the relative response $[v(t)-u(L,t)]$ superimposed to the FEP of the hamiltonian system.
9. HHT analysis of the NES response, Stage I of the damped transition of Figure 8: (a) Instantaneous frequency of the 1st IMF superimposed to the wavelet transform of the transient response; (b) Reconstruction of the transient response using the 1st IMF.
10. HHT analysis of the rod end response, Stage I of the damped transition of Figure 8: (a) Instantaneous frequencies of the 1st and 2nd IMF superimposed to the wavelet transform of the transient response; (b) Reconstruction of the transient response using the 1st and 2nd IMF.
11. HHT analysis of the NES response, Stage II of the damped transition of Figure 8: (a) Instantaneous frequency of the 1st IMF superimposed to the wavelet transform of the transient response; (b) Reconstruction of the transient response using the 1st IMF.
12. HHT analysis of the rod end response, Stage II of the damped transition of Figure 8: (a) Instantaneous frequencies of the 1st, 2nd and 3rd IMF superimposed to the wavelet transform of the transient response; (b) Reconstruction of the transient response using the 1st, 2nd and 3rd IMF.
13. HHT analysis of the NES response, Stages III and IV of the damped transition of Figure 8: Instantaneous frequencies (superimposed on the wavelet transform of the response), and time series of the (dominant) 3rd, 4th and 5th IMFs.
14. HHT analysis of the NES response, Stages III and IV of the damped transition of Figure 8: Reconstruction of the response by superposing the three dominant IMFs.
15. HHT analysis of the rod end response, Stages III and IV of the damped transition of Figure 8: (a) Instantaneous frequencies (superimposed on the wavelet transform of the response) of the (dominant) 1rd, 2nd, 3rd and 4th IMF, (b) Reconstruction of the response by superposing the four dominant IMFs.

Figures

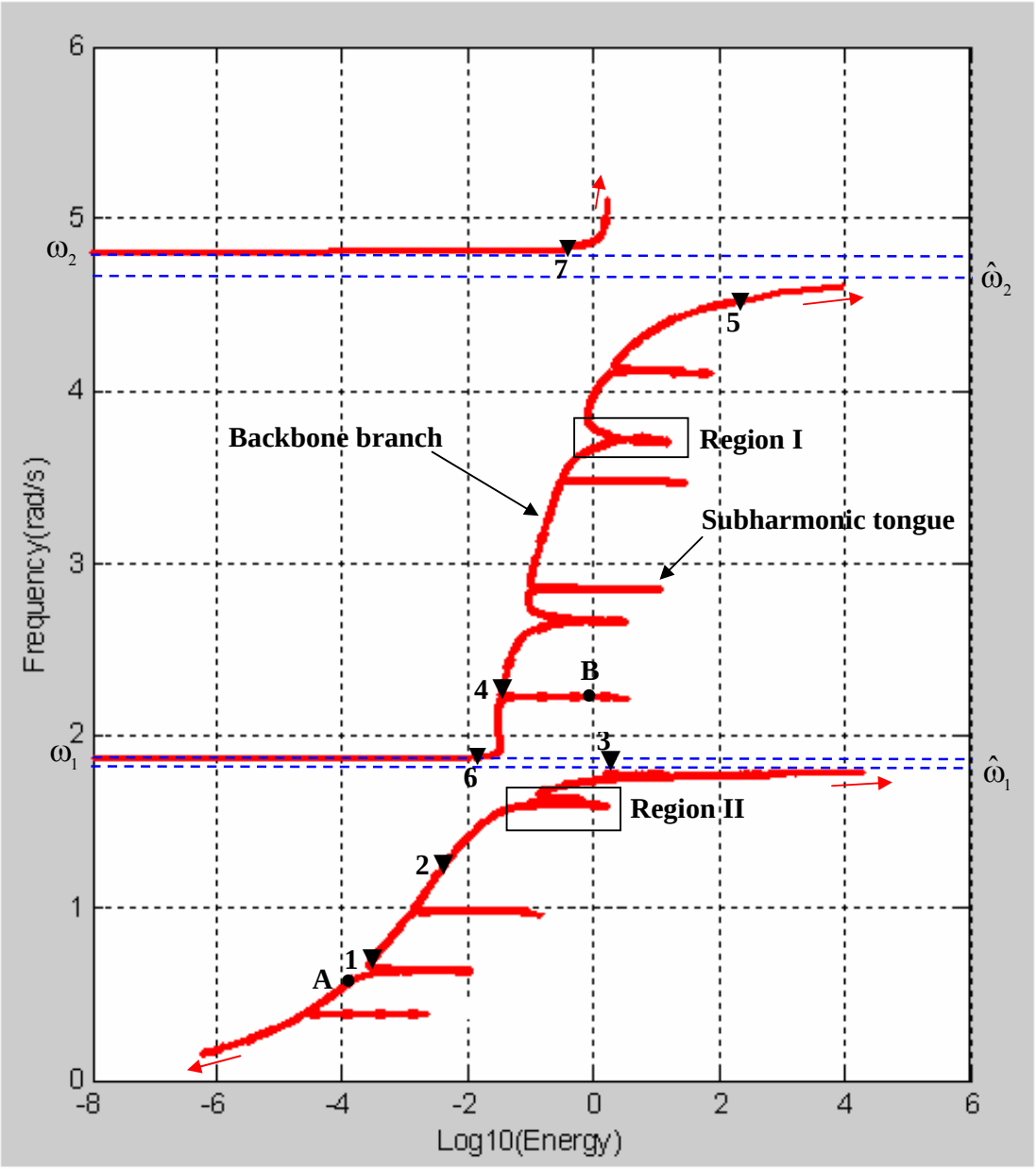
Backbone branch
Region I
Subharmonic tongue
Region II
A
B
1
2
3
4
5
6
7
ω_2
ω_1
$\hat{\omega}_2$
$\hat{\omega}_1$
Frequency(rad/s)
Log10(Energy)

(a)

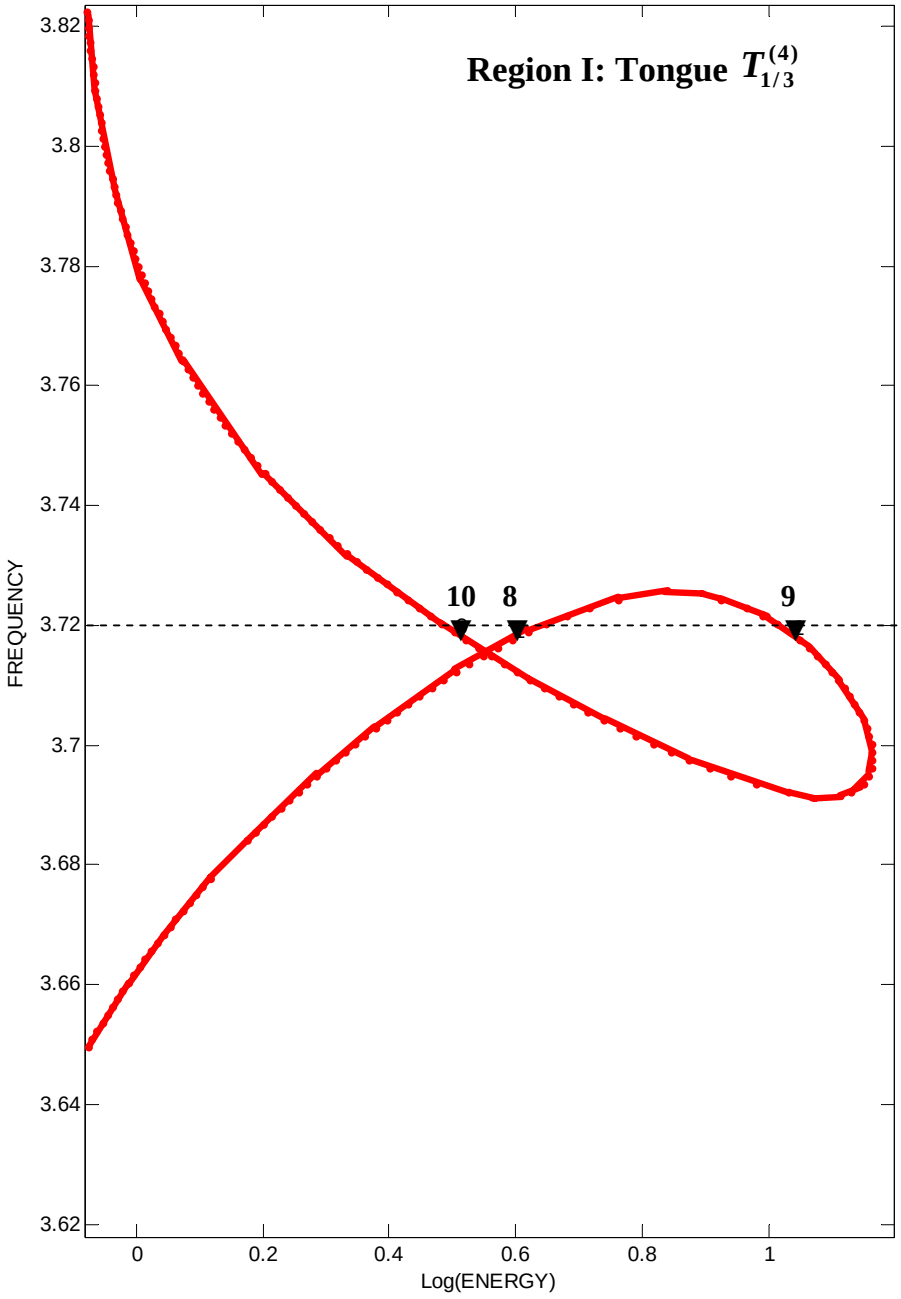
Region I: Tongue $T_{1/3}^{(4)}$
10
8
9
FREQUENCY
Log(ENERGY)
3.82
3.8
3.78
3.76
3.74
3.72
3.7
3.68
3.66
3.64
3.62
0
0.2
0.4
0.6
0.8
1

(b)

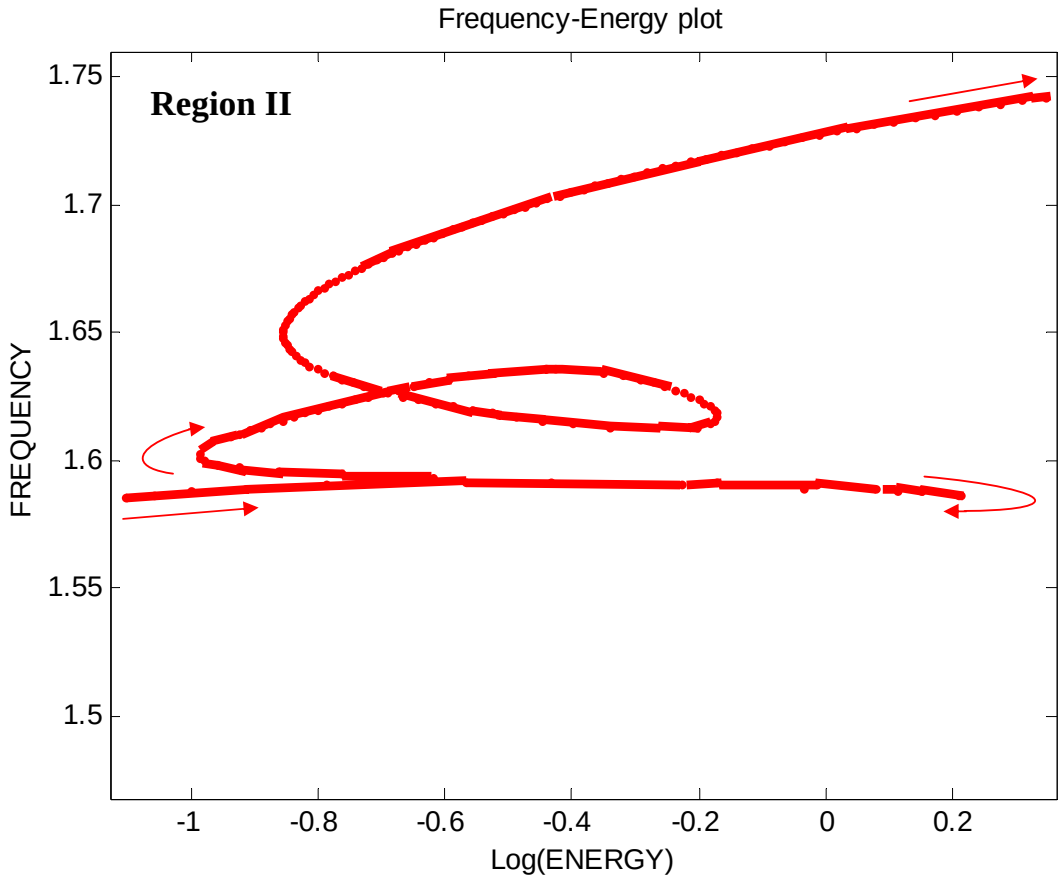
Frequency-Energy plot
Region II
1.75
1.7
1.65
1.6
1.55
1.5
FREQUENCY
-1
-0.8
-0.6
-0.4
-0.2
0
0.2
Log(ENERGY)

(c)

Figure 1

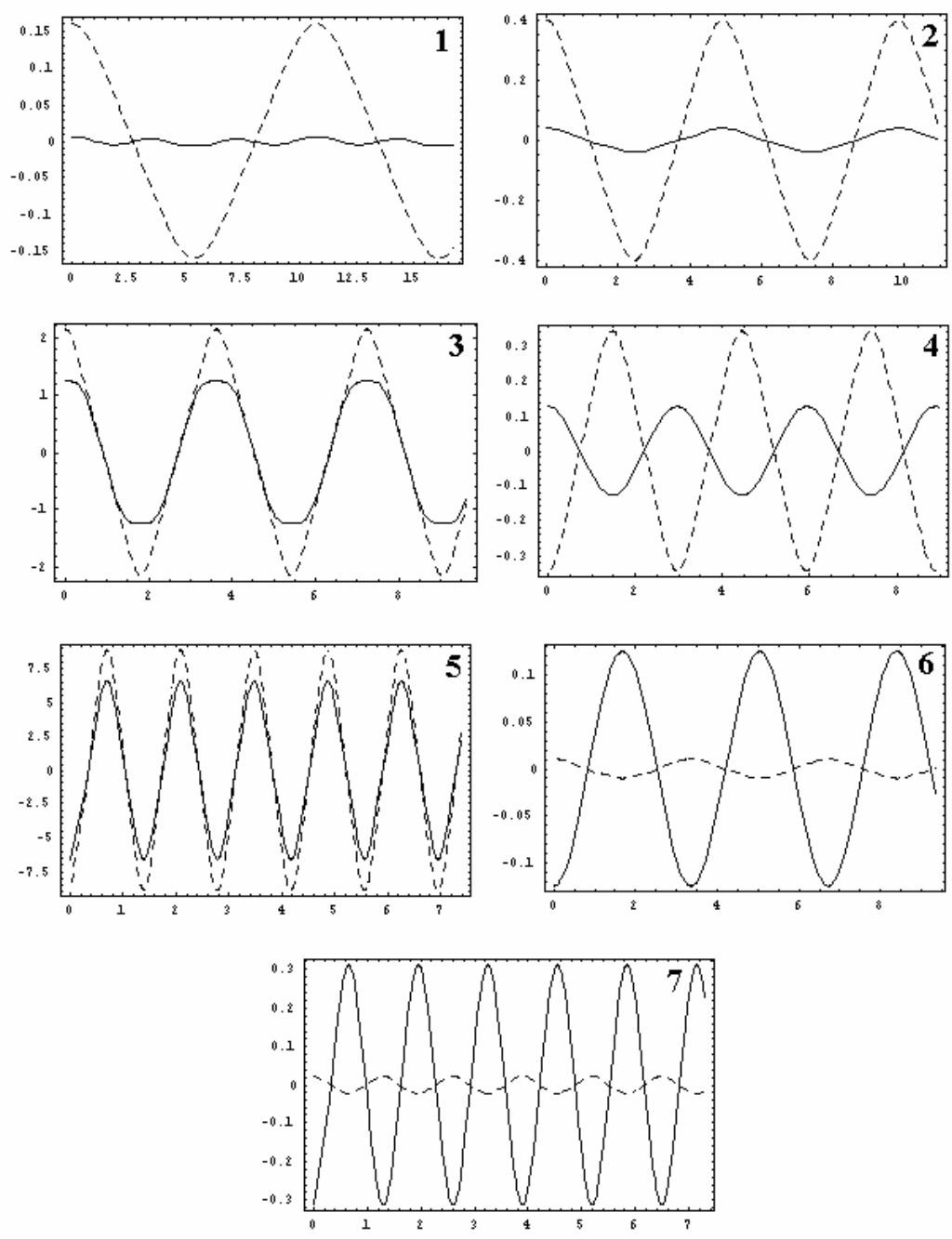

Figure 2

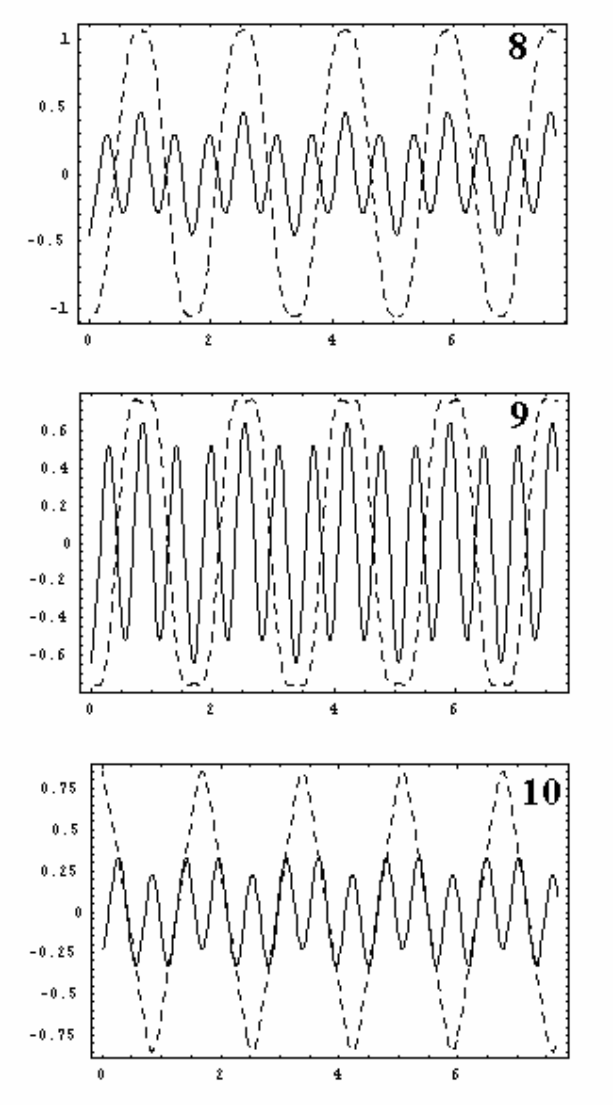
8
1
0.5
0
-0.5
-1
0
2
4
6
9
0.6
0.4
0.2
0
-0.2
-0.4
-0.6
0
2
4
6
10
0.75
0.5
0.25
0
-0.25
-0.5
-0.75
0
2
4
6

Figure 3

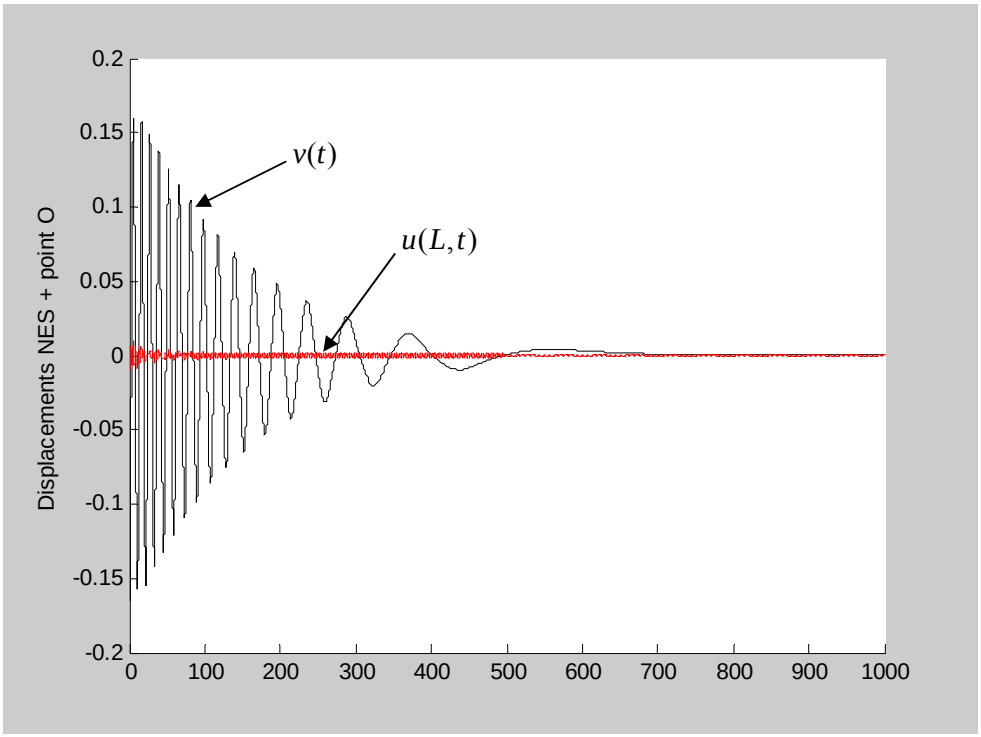
Displacements NES + point O
v(t)
u(L,t)
0.2
0.15
0.1
0.05
0
-0.05
-0.1
-0.15
-0.2
0
100
200
300
400
500
600
700
800
900
1000

(a)

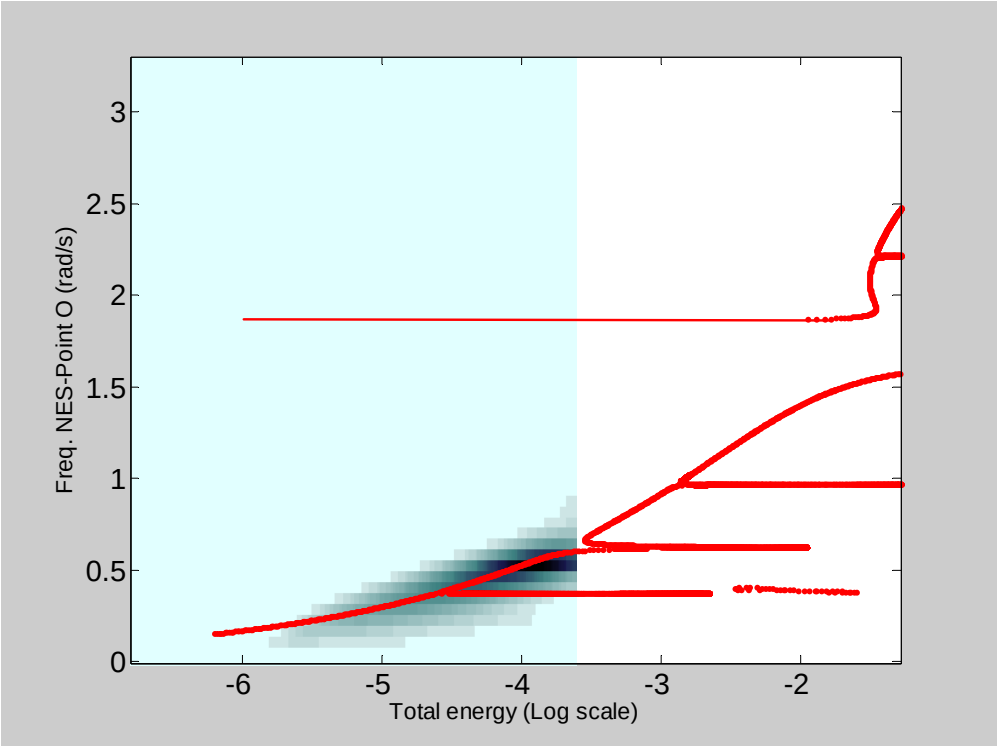
Freq. NES-Point O (rad/s)
Total energy (Log scale)
3
2.5
2
1.5
1
0.5
0
-6
-5
-4
-3
-2

(b)

Figure 4

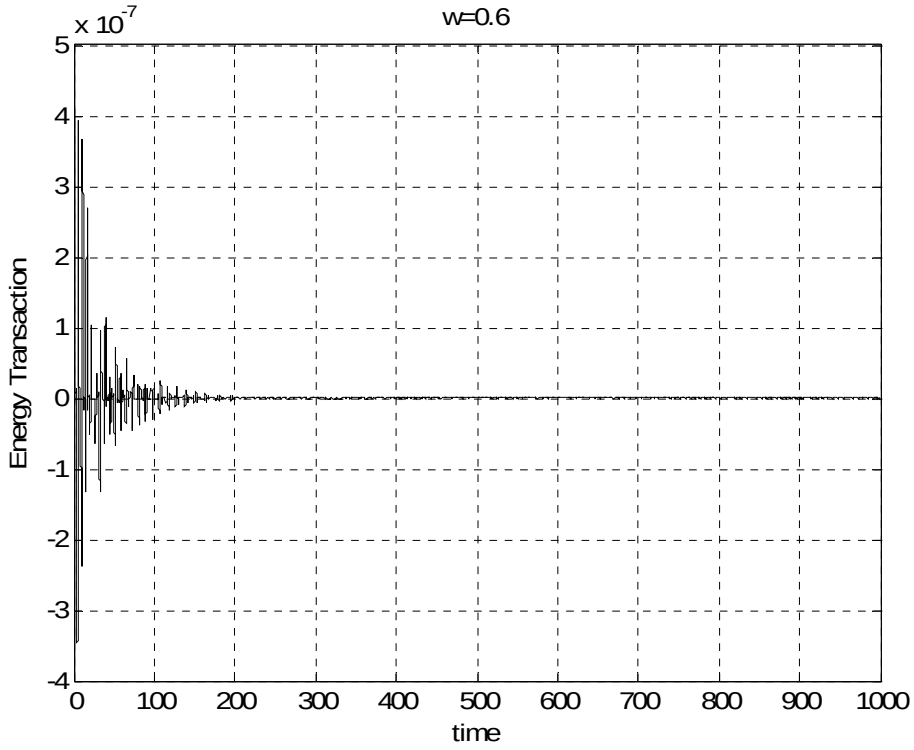
x 10^-7
w=0.6
Energy Transaction
time
5
4
3
2
1
0
-1
-2
-3
-4
0
100
200
300
400
500
600
700
800
900
1000

Figure 5

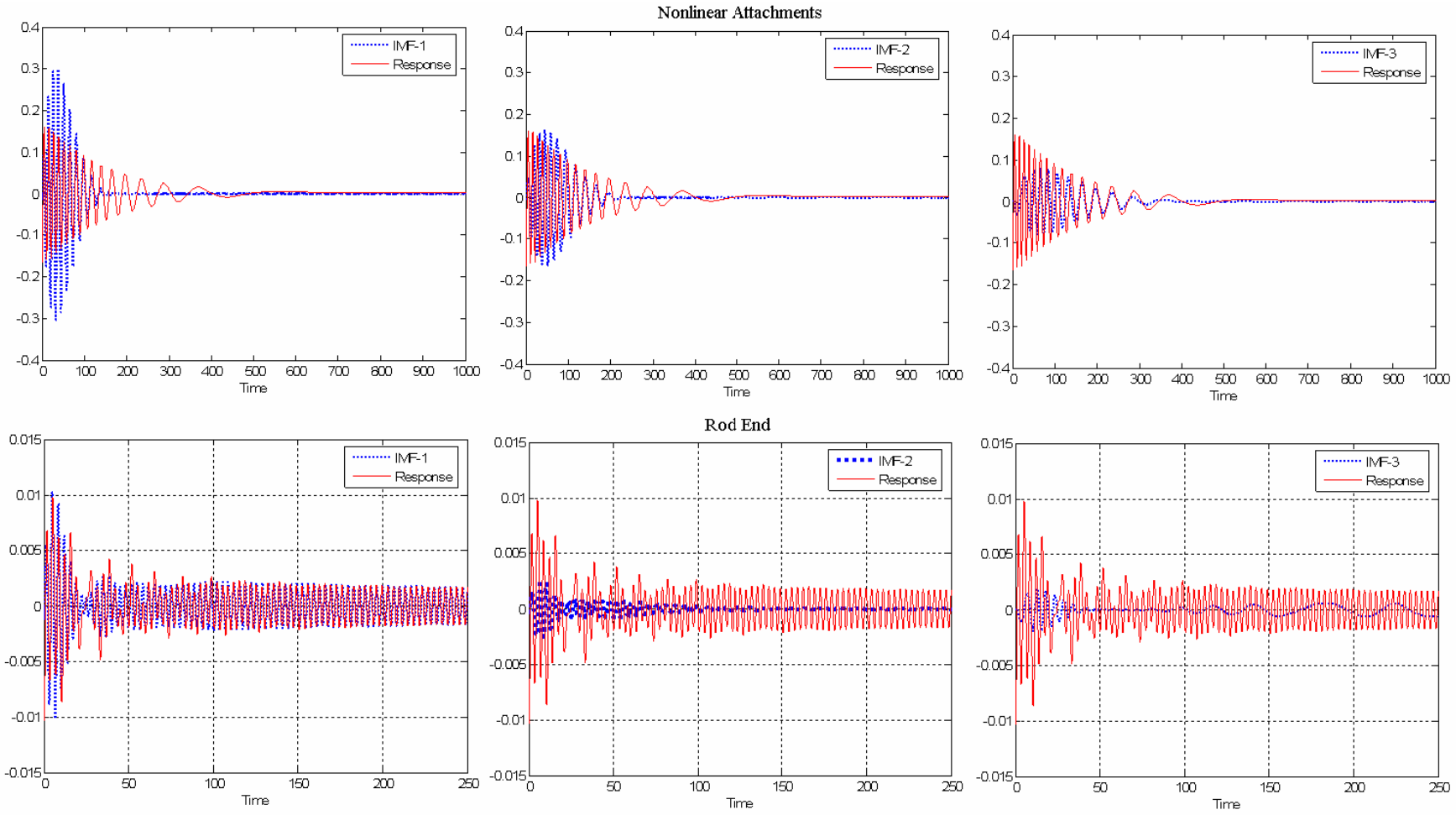
Nonlinear Attachments
IMF-1
Response
IMF-2
Response
IMF-3
Response
Time
Rod End
IMF-1
Response
IMF-2
Response
IMF-3
Response
Time

Figure 6

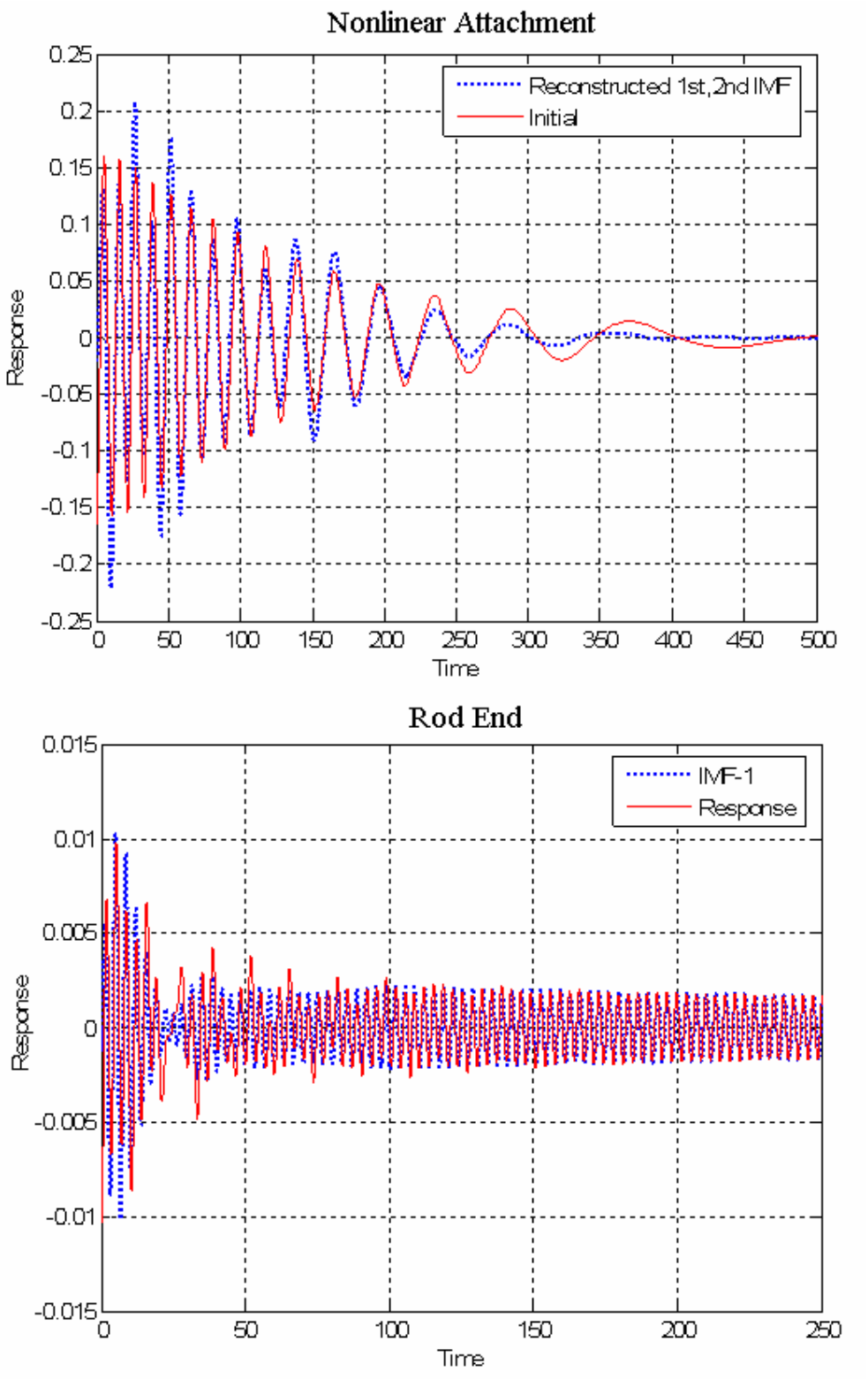
Nonlinear Attachment
Reconstructed 1st,2nd IMF
Initial
Response
Time
Rod End
IMF-1
Response
Response
Time

Figure 7

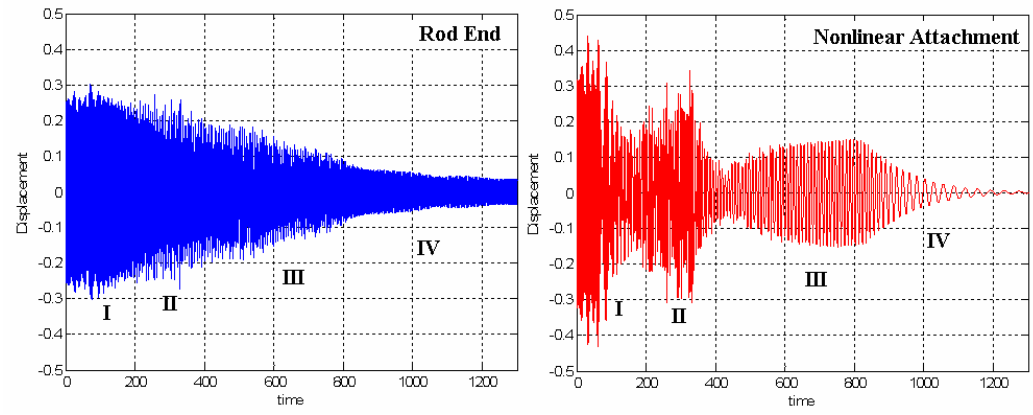
Rod End
Nonlinear Attachment
Displacement
time
I
II
III
IV

(a)

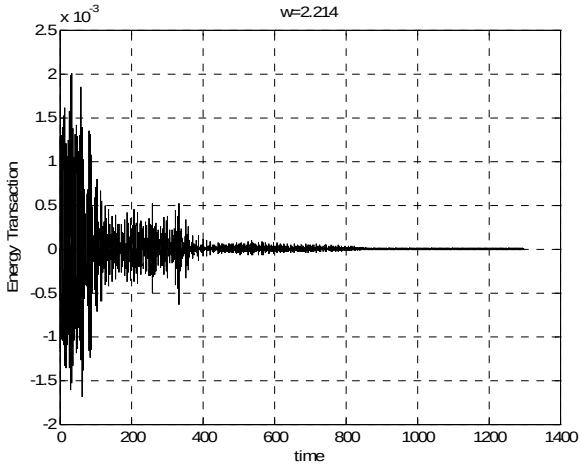
x 10^-3
w=2.214
Energy Transaction
time

(b)

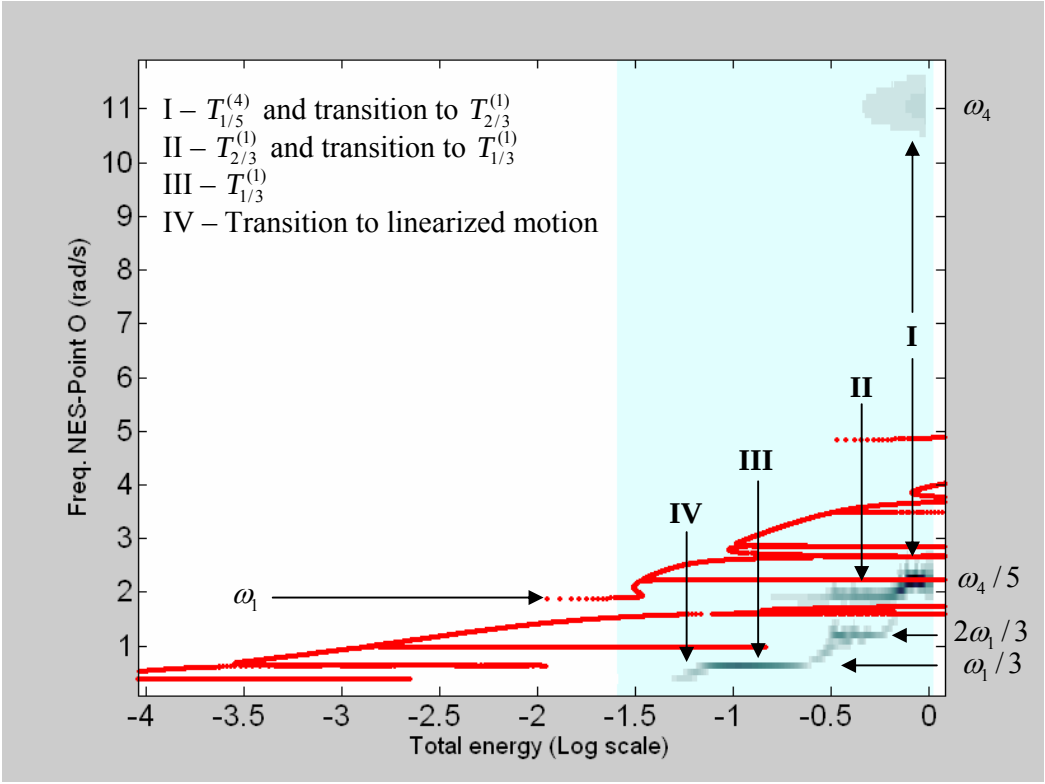
I – $T_{1/5}^{(4)}$ and transition to $T_{2/3}^{(1)}$
II – $T_{2/3}^{(1)}$ and transition to $T_{1/3}^{(1)}$
III – $T_{1/3}^{(1)}$
IV – Transition to linearized motion
Freq. NES-Point O (rad/s)
Total energy (Log scale)
ω_4
$\omega_4/5$
$2\omega_1/3$
$\omega_1/3$
ω_1

(c)

Figure 8

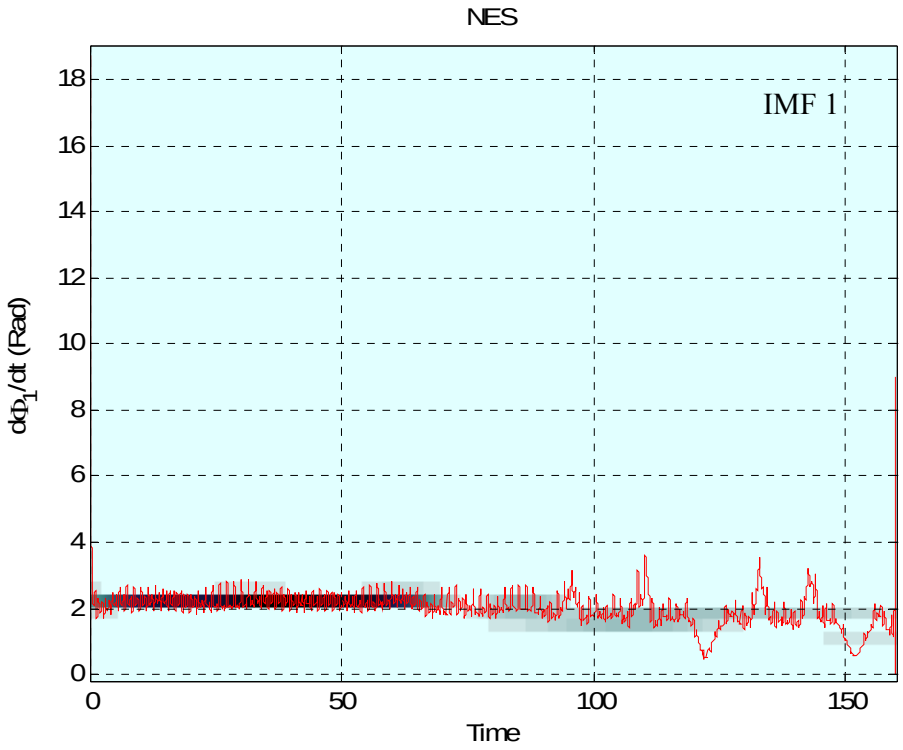
NES
IMF 1
dφ1/dt (Rad)
Time
0
2
4
6
8
10
12
14
16
18
0
50
100
150

(a)

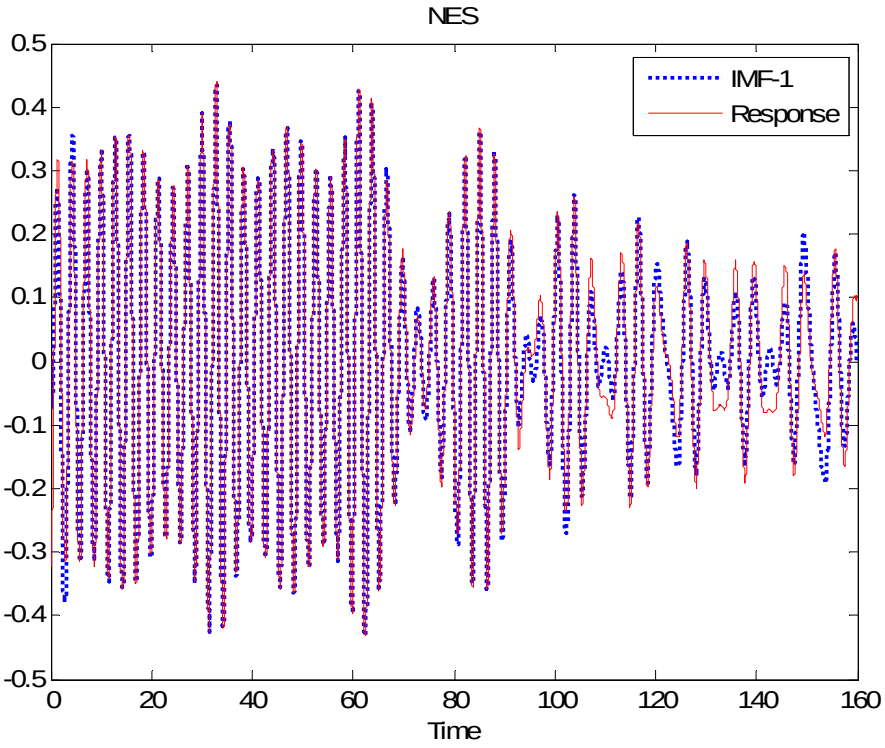
NES
IMF-1
Response
Time
0.5
0.4
0.3
0.2
0.1
0
-0.1
-0.2
-0.3
-0.4
-0.5
0
20
40
60
80
100
120
140
160

(b)

Figure 9

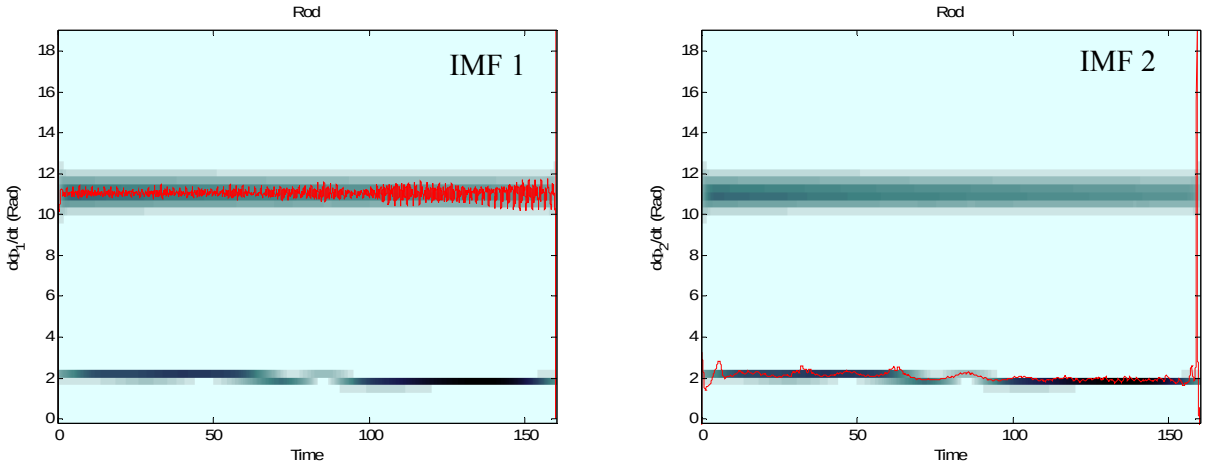
Rod
IMF 1
dθ1/dt (Rad)
Time
Rod
IMF 2
dθ2/dt (Rad)
Time

(a)

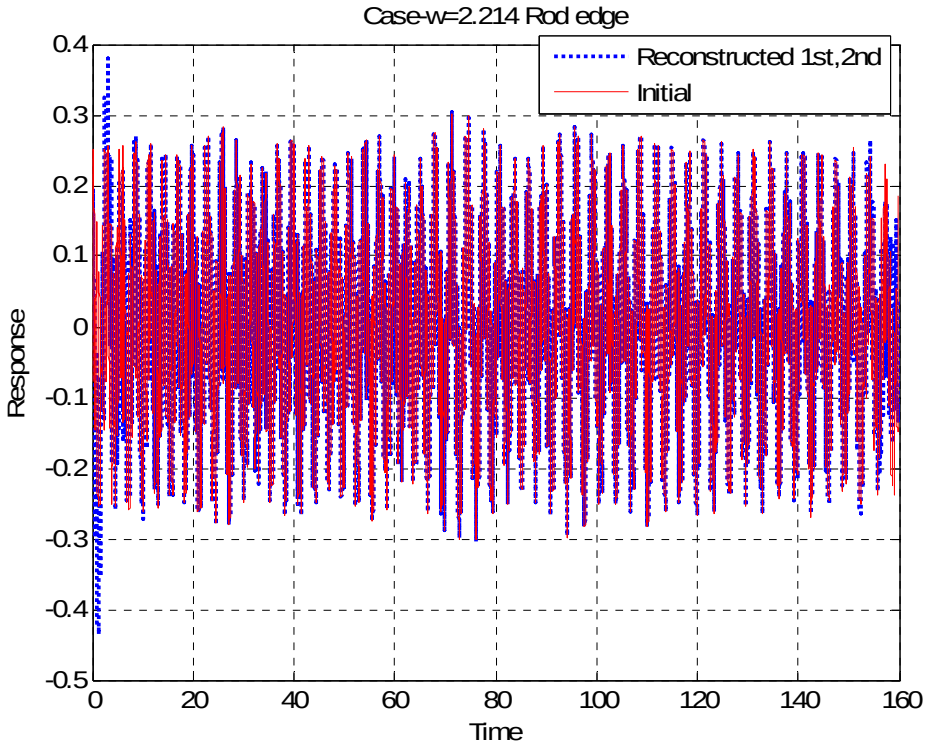
Case-w=2.214 Rod edge
Reconstructed 1st,2nd
Initial
Response
Time

(b)

Figure 10

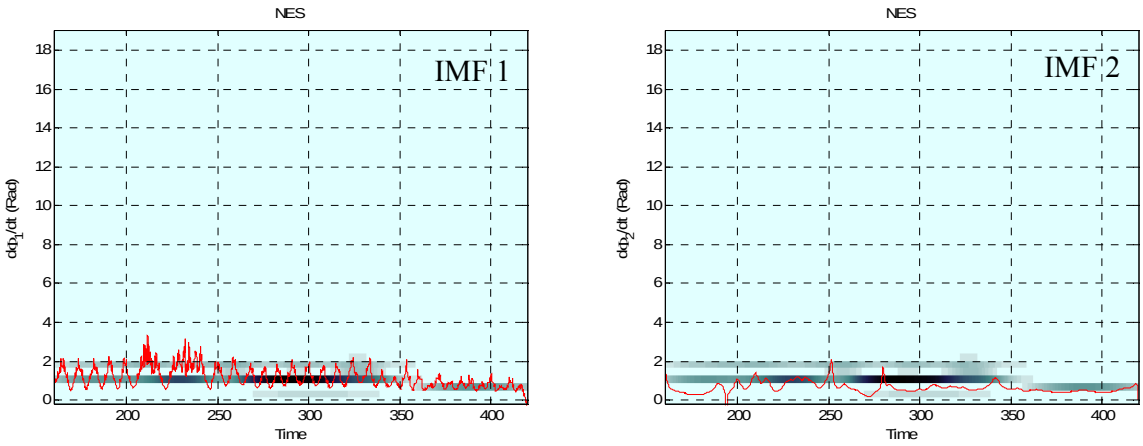
NES
IMF 1
NES
IMF 2
Time
Time

(a)

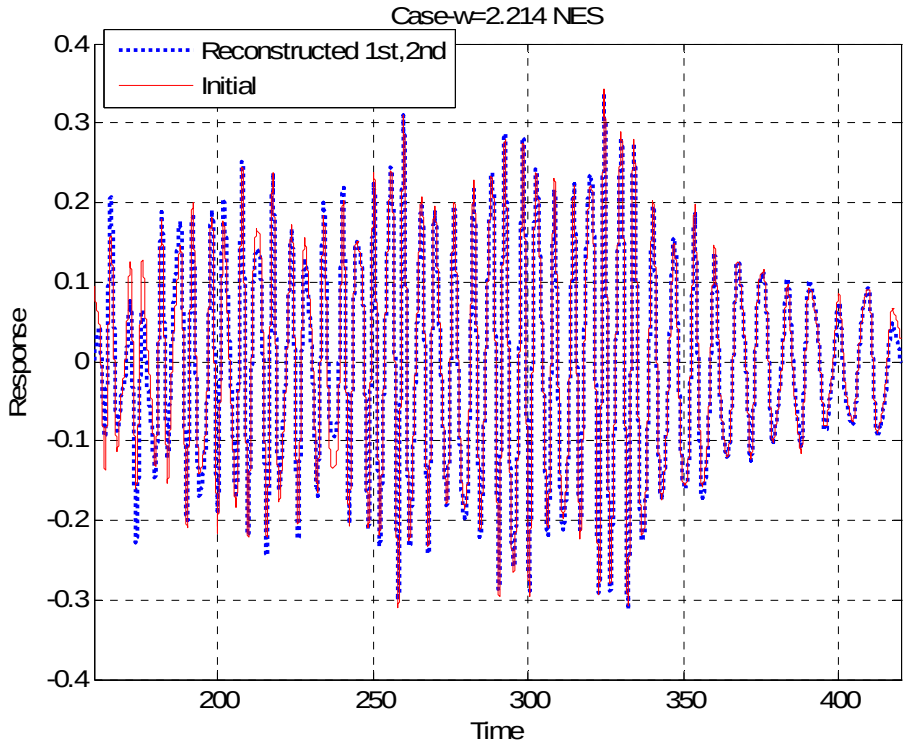
Case-w=2.214 NES
Reconstructed 1st,2nd
Initial
Response
Time

(b)

Figure 11

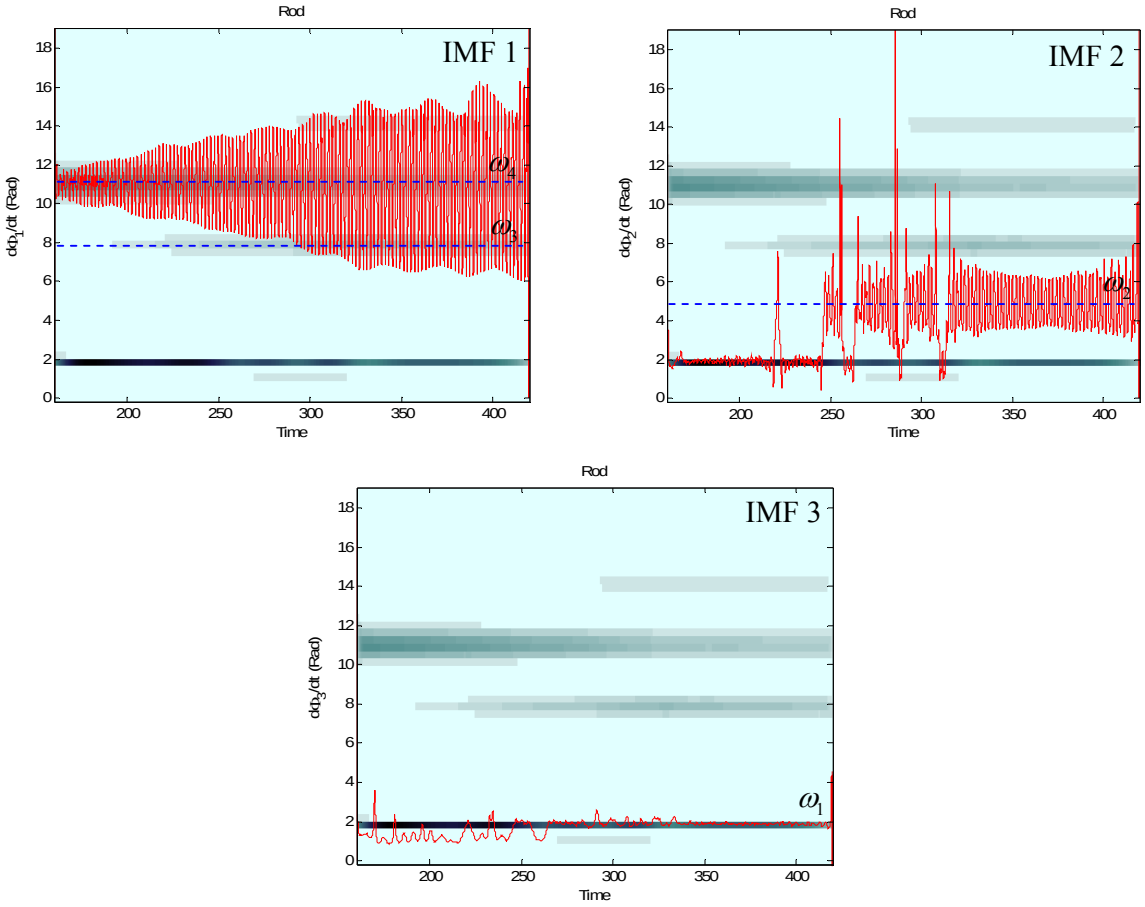
Rod
IMF 1
ω_4
ω_3
$d\theta_1/dt$ (Rad)
Time
Rod
IMF 2
ω_2
$d\theta_2/dt$ (Rad)
Time
Rod
IMF 3
ω_1
$d\theta_3/dt$ (Rad)
Time

(a)

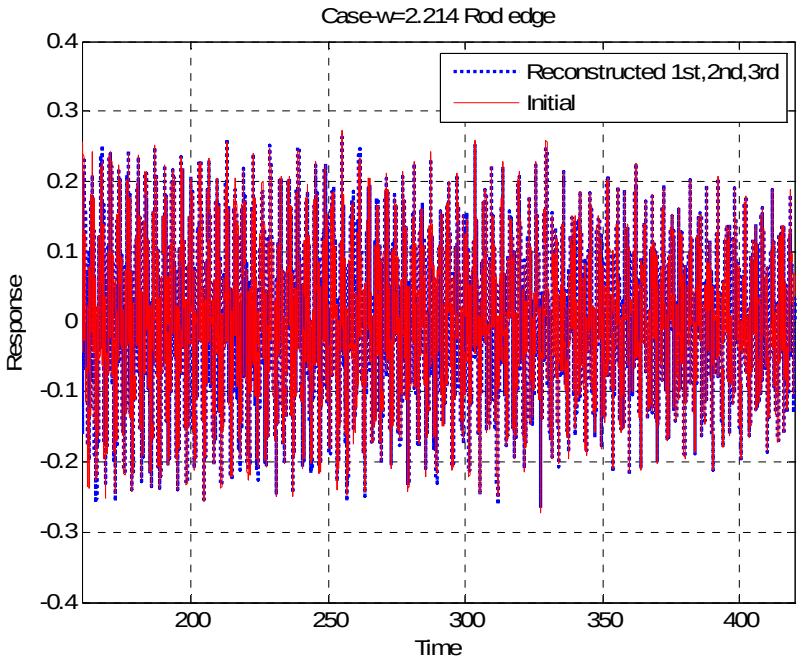
Case-w=2.214 Rod edge
Reconstructed 1st,2nd,3rd
Initial
Response
Time

(b)

Figure 12

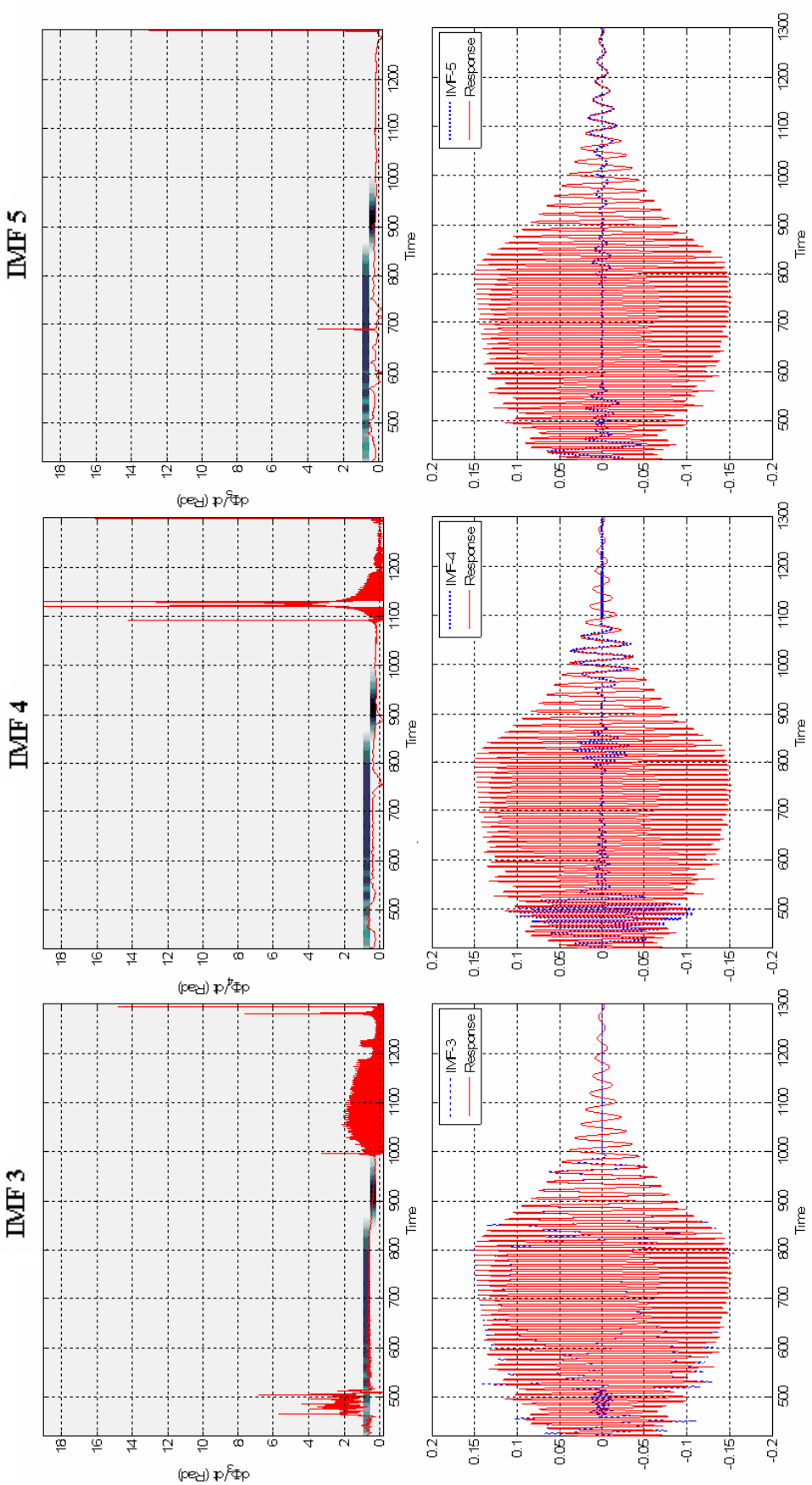
IMF 3
IMF 4
IMF 5
dΦ3/dt (Rad)
dΦ4/dt (Rad)
dΦ5/dt (Rad)
Time
IMF-3
IMF-4
IMF-5
Response

Figure 13

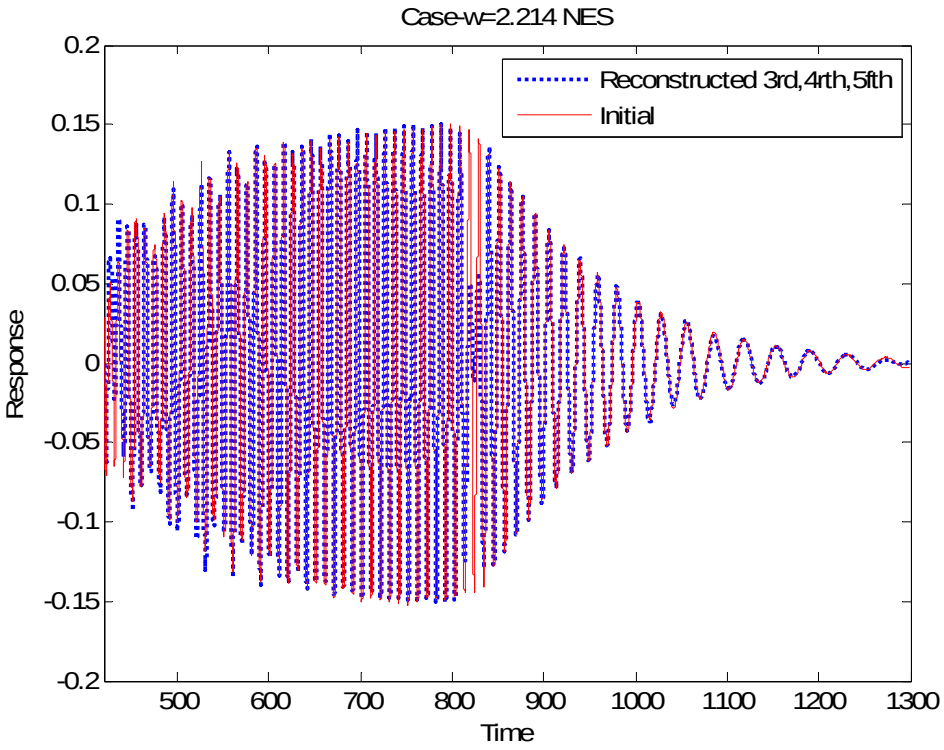
Case-w=2.214 NES
Reconstructed 3rd,4rth,5fth
Initial
Response
Time
0.2
0.15
0.1
0.05
0
-0.05
-0.1
-0.15
-0.2
500
600
700
800
900
1000
1100
1200
1300

Figure 14

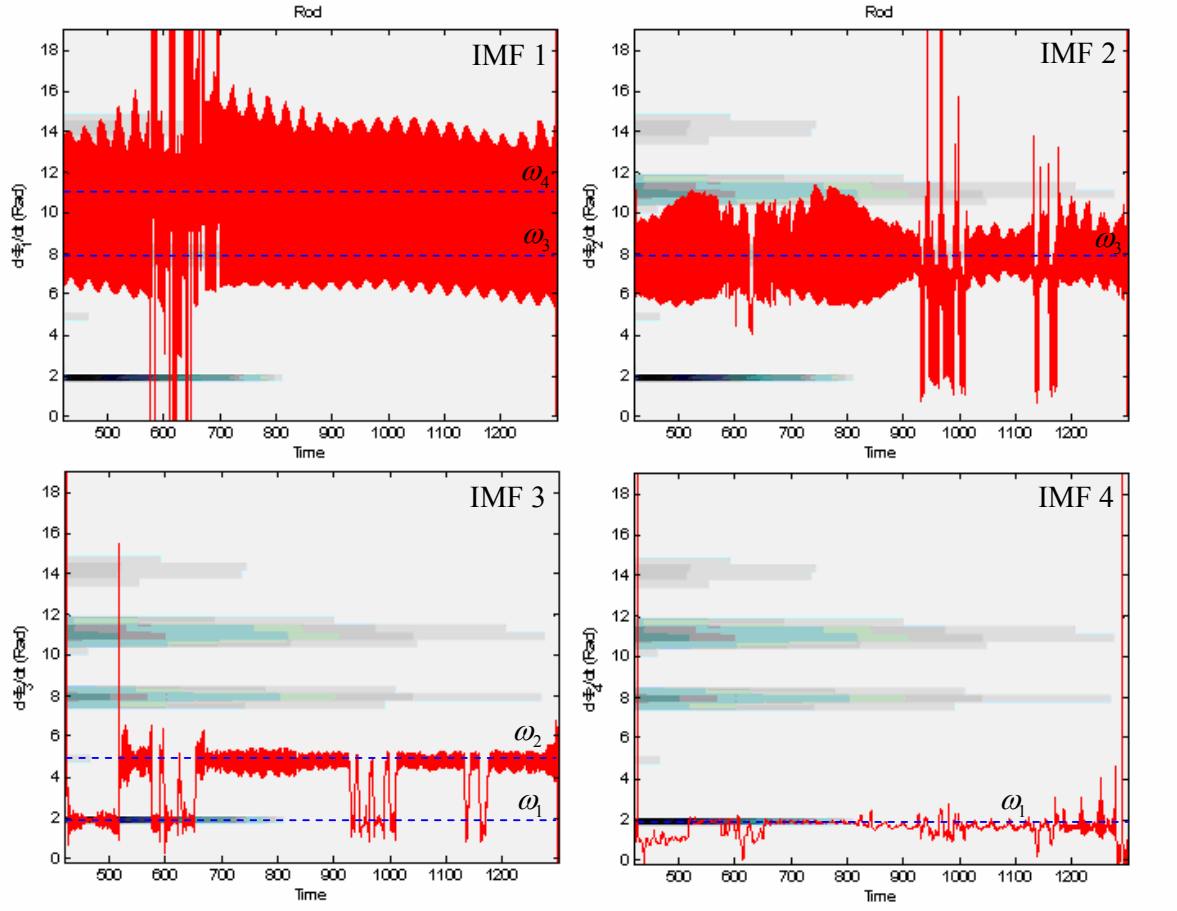
Rod
IMF 1
IMF 2
IMF 3
IMF 4
Time
ω_4
ω_3
ω_2
ω_1

(a)

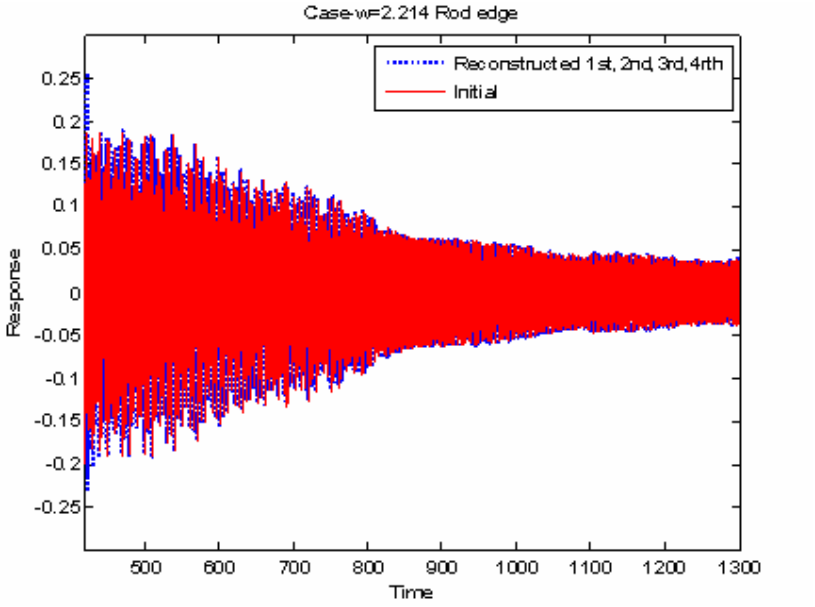
Case-w=2.214 Rod edge
Reconstructed 1st, 2nd, 3rd, 4rth
Initial
Response
Time

(b)

Figure 15